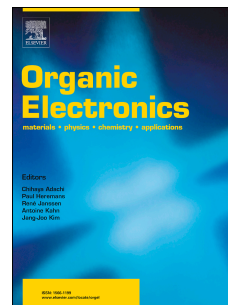


Accepted Manuscript

Novel A-D-A type small molecules with β -alkynylated BODIPY flanks for bulk heterojunction solar cells

Junxu Liao, Yongjun Xu, Hongbin Zhao, Qiao Zong, Yutang Fang



PII: S1566-1199(17)30311-7

DOI: [10.1016/j.orgel.2017.06.054](https://doi.org/10.1016/j.orgel.2017.06.054)

Reference: ORGELE 4179

To appear in: *Organic Electronics*

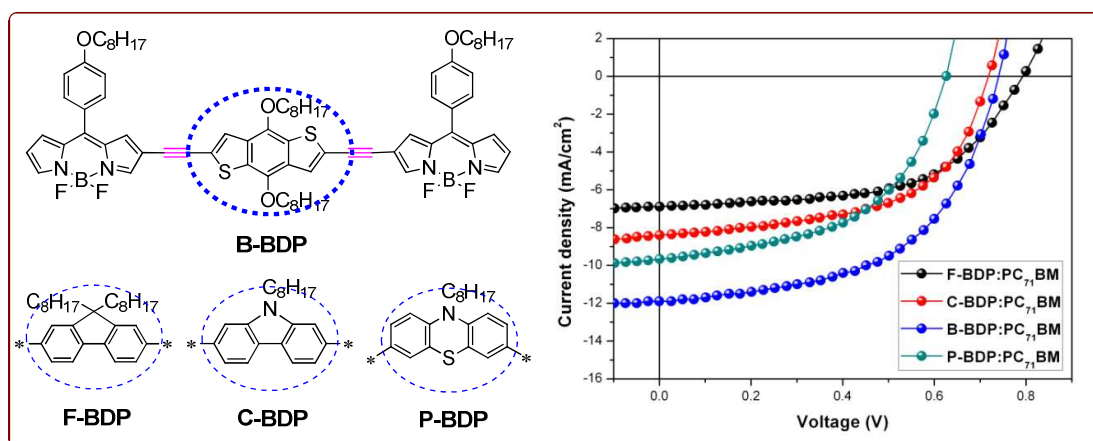
Received Date: 11 April 2017

Revised Date: 19 June 2017

Accepted Date: 20 June 2017

Please cite this article as: J. Liao, Y. Xu, H. Zhao, Q. Zong, Y. Fang, Novel A-D-A type small molecules with β -alkynylated BODIPY flanks for bulk heterojunction solar cells, *Organic Electronics* (2017), doi: 10.1016/j.orgel.2017.06.054.

This is a PDF file of an unedited manuscript that has been accepted for publication. As a service to our customers we are providing this early version of the manuscript. The manuscript will undergo copyediting, typesetting, and review of the resulting proof before it is published in its final form. Please note that during the production process errors may be discovered which could affect the content, and all legal disclaimers that apply to the journal pertain.



Four A-D-A type BODIPY derivatives with ethynyl bridges were designed and synthesized for small molecule organic solar cells (SM-OSCs). All these molecules show appealing photovoltaic performance. Among them, **B-BDP/PC₇₁BM** based OSC exhibit not only good photoelectric characteristic but also superior charge transport property and favorable nanoscale morphology relative to the other counterparts and thus pronounce to a higher PCE of 4.65% with a J_{sc} of 11.84 mA cm² and a FF of 53.8%, which is one of the best values in BODIPY based OSCs.

Novel A-D-A type small molecules with β -alkynylated BODIPY flanks for bulk heterojunction solar cells

Junxu Liao^{a, b}, Yongjun Xu^{a, *}, Hongbin Zhao^{a, *}, Qiao Zong^a, and Yutang Fang^b

^a School of Chemical Engineering and Energy Technology, Dongguan University of Technology, Dongguan 523808, People's Republic of China

^b School of Chemistry and Chemical Engineering, South China University of Technology, Guangzhou 510641, People's Republic of China

Abstract:

A series of novel A-D-A type small molecules with BODIPY linked through alkynyl with various electron donor units such as fluorene, carbazole, benzodithiophene and phenothiazine, namely **F-BDP**, **C-BDP**, **B-BDP** and **P-BDP**, respectively, were designed and synthesized. Introducing the alkynyl bridge leads to extending the molecular absorption spectrum to the range of 320-700 nm with high molar extinction coefficients ($10^5 \text{ cm}^{-1} \text{ M}^{-1}$) and strong fluorescence quenching. The molecules showed relatively low HOMO ranging from -5.02 to -5.24 eV as estimated from cyclic voltammetry measurements. Interestingly, **B-BDP** with BDT as donor exhibits more obviously red-shifted absorption in the solid state compared to **F-BDP**, **C-BDP** and **P-BDP**. Furthermore, the solution-processed bulk-heterojunction organic solar cell based on **B-BDP**/PC₇₁BM present superior charge transport property and more favorable nanoscale morphology, resulting in a significant higher J_{sc} of 11.84 mA cm^{-2} and FF than the other counterparts, thus achieved a higher

* Corresponding author. Tel.: +86-139-2583-6155; fax: +86-769-2286-2605; e-mail: hnllxyj@126.com.

* Corresponding author. Tel.: +86-158-1831-8389; fax: +86-769-2286-2601; e-mail: zhaohbhanlf@163.com.

PCE of 4.65%, which is one of the best values among the ever reported BODIPY based organic solar cells.

Keywords: BODIPY derivatives, organic solar cells, acceptor-donor-acceptor, optoelectronic properties, DFT calculations, photovoltaic performances

1. Introduction

Solution-processed bulk heterojunction (BHJ) organic solar cells (OSCs) are promising to solve the growing energy crisis and environmental deterioration worldwide. In the past decades, BHJ-OSCs have attracted enormous attention due to the advantages of low-cost, light-weight, and flexibility [1-5]. Depending on the molecular weight, the organic semiconductors used in OSCs can be either polymers or π -conjugated small molecules (SMs), both of which have achieved remarkable power conversion efficiencies (PCE) of over 10% in single-junction devices [6-11]. In comparison with polymer counterparts, SMs present many additional merits such as well-defined molecular structures, low molecular weight, simple purification and superior batch-to-batch reproducibility, and have the potential to produce low-cost and large-scale OSCs for commercial applications in the near future [12-13], and there is a wide scope to enhance the PCE of BHJ-OSCs based on SMs.

In the small molecule based organic solar cells (SM-OSCs), for achieving high efficiency photovoltaic properties, the donor materials should be tailored to combine the following characteristics: (i) relatively low optical absorption band gaps and high absorption coefficients to guarantee efficient photo-response [14-16], (ii) suitable energy level offsets with a fullerene acceptor to ensure efficient charge separation [17-20], (iii) extended π -electron delocalization and backbone planarity to lead to high charge mobility [21-22]. A common method to develop

efficient photovoltaic materials with high light harvesting ability is construction of narrow band gap molecules by using donor-acceptor (D-A) structure [2, 23-24]. Another strategy to promote molecular light harvesting ability in OSCs is introducing the dye building blocks such as rhodanine [25-28], DPP [29-32], porphyrin [33-36], and so on [37].

4,4-difluoro-4-bora-3a,4a-diaza-s-indacene (BODIPY) have proved to be highly versatile dyes owing to their remarkable photophysical properties including strong ground-state absorption, outstanding redox activity, intense fluorescent emission, high photoluminescence quantum yield and excellent chemical stability [38-39]. Moreover, BODIPY can be easily tailored by chemical transformation and their photophysical properties can be readily tuned by structural modifications at the periphery and at the boron atom of the BODIPY skeleton [40-43], which provide additional opportunities to meet the different requirements for diverse applications. Roncali et al. reported the first examples of BODIPY donors involving two styryl units along with PC₆₁BM as the electron acceptor for solution-processed BHJ-OSCs [44]. Subsequently, other groups reported some BHJ-OSCs based on BODIPY SMs and polymers [45-49]. In 2016, our group reported a series of D-A-D type BODIPY derivatives with various electron donors at 2,6-positions for BHJ-OSCs, and the best device exhibits 2.15% PCE [50]. Sharma et al. have demonstrated the high efficiency OSCs with alkynyl carbazole modified BODIPY derivatives as the donor materials, which marked one of the significant advances of this dye family's applications [51]. Very recently, Bulut et al. reported a BODIPY dye, BET, with triazatruxene groups linked at 2,6-positions of BODIPY core through alkynyl bridge. An encouraging PCE of 5.8%, with a high FF of 65%, was achieved in BHJ-OSCs [52]. However, although BODIPY derivatives showed great potential as donor materials for OSCs, to date, the best PCE based on BODIPY were in 4.7%-6% range

[44-52], which are moderate values in SM-OSCs. This is mainly due to the fact that the photovoltaic materials based on BODIPY derivatives have not been fully developed, leading to the high-performance devices are still rare. Thus, exploring novel excellent BODIPY based photovoltaic materials is challengeable and is urgently needed.

In BODIPY based SM-OSCs, the device performance is often limited by the inappropriate molecular structure and the unfavorable morphology. To overcome these shortcomings and exploit novel high-efficiency materials, in this work, we design and synthesize four A-D-A type small molecules with BODIPY linked through alkynyl with various electron donor units such as fluorene, carbazole, benzodithiophene and phenothiazine, namely **F-BDP**, **C-BDP**, **B-BDP** and **P-BDP**, respectively (Chart 1). The molecular design rationale is as follow: First, introducing ethynyl can effectively reduce the dihedral angle between the electron donor and BODIPY core, consequently achieve a coplanar structure. The coplanar molecular geometry is expected to contribute to greater crystallinity, improved charge transport, and a lower band gap of the semiconductor. Second, BODIPY intrinsically possess strong electronegativity and intense absorption. Considering that fluorene [53], carbazole [53], benzodithiophene [54] and phenothiazine [55] are excellent electron-rich building blocks in the organic photoelectric material, the designed D-A-D molecules are supposed to induce intramolecular charge transfer and lead to broad and strong absorption throughout the visible and even NIR region. Third, compared with fluorene and carbazole, S containing benzodithiophene and phenothiazine have the ability to form additional intermolecular non-covalent S...S band to strengthen the intermolecular interaction, which induce positive effects on electronic properties, charge transport, film morphology, and photovoltaic properties. With this comparative series, we are able to investigate these effects. The

thermal stability, physical properties, and electrochemical behavior of these SMs are systematically studied. The BHJ-OSC devices using the new BODIPY derivatives as electron donors combined with [6,6]-phenyl-C₇₁-butyric acid methyl ester (PC₇₁BM) as electron acceptor are fabricated and their photovoltaic performances are investigated to insight their potential photovoltaic applications. Significant effect of central electron donating units on these opto-electronic properties was observed in these SMs. The best photovoltaic performance with a PCE of 4.65% and a short circuit current density of 11.84 mA cm² were obtained in the **B-BDP** based OSCs.

2. Experimental section

2.1 Materials

4-hydroxybenzaldehyde, 2,7-dibromo-9H-fluorene, 3,6-dibromo-9H-carbazole, pyrrole, iodine chloride, 1-bromooctane, trimethylsilylacetylene, bis(triphenylphosphine)palladium(II)dichloride, copper(I) iodide, indium(III) chloride, 4,4,4',4',5,5,5',5'-octamethyl-2,2'-di(1,3,2-dioxaborolane), boron trifluoride ether complex and 4,5-dichloro-3,6-dioxocyclohexa-1,4-diene-1,2-dicarbonitrile (TCQ) were purchased from commercial sources. 4,8-bis(octyloxy)benzo[1,2-b:4,5-b']dithiophene (**11**) and 10-octyl-10H-phenothiazine (**15**) were prepared as described in the literature [56-57]. Pyrrole was distilled from CaH₂ before use. THF and toluene were dried and distilled over sodium and benzophenone. Dichloromethane and methanol were dried under 4A molecular sieves. Column chromatography was performed on silica (300-400 mesh).

2.2 Characterization and measurement

¹H NMR and ¹³C NMR spectra were recorded on a Bruker Avance spectrometer (600 and 151

MHz, respectively) with tetramethylsilane (TMS, 0 ppm) as the internal standard using CDCl_3 as solvent. Matrix-assisted laser desorption/ionization time of flight mass spectra (MALDI-TOF-MS) were recorded on a Bruker ultraflex-II spectrometer using α -cyano-4-hydroxyl-cinnamic acid (α -CHCA) matrix. High resolution mass spectra (HRMS) were recorded on an Agilent 6530 Accurate Mass Q-TOF LC-MS instrument. Thermogravimetric analysis (TGA) was carried out using a Netzsch TG 209 analyzer at a heating rate of $10\text{ }^\circ\text{C min}^{-1}$ up to $600\text{ }^\circ\text{C}$. Differential scanning calorimetry (DSC) was recorded on a NETZSCH DSC 200F3 instrument. UV-vis absorption spectra were collected on an SHIMADZU UV-2550 UV-vis spectrophotometer and emission spectra were recorded by using a Hitachi F-4500 instrument. Emission spectra were fully corrected by reference to a standard lamp. Cyclic voltammetric (CV) was carried out on a CHI660E electrochemical workstation utilizing the three electrode configuration consisting of a gold electrode (working electrode), platinum wire (auxillary electrode) and Ag/AgCl electrode (reference electrode). The experiments were carried out in CH_2Cl_2 solution using 0.1 M tetrabutylammonium hexafluorophosphate ($n\text{-Bu}_4\text{NPF}_6$) as supporting electrolyte. The solution was deoxygenated at room temperature under nitrogen protection. The transmission electron microscope (TEM) was carried out on a FEI Tecnai T20 instrument. X-ray diffraction (XRD) experiments were performed on a Rigaku D/max-2500 X-ray diffractometer. The theoretical study was performed on the 6-31G** basis set in Gaussian09 using the density functional theory (DFT), as approximated by the B3LYP.

2.3 Fabrication and characterization of the photovoltaic cells

Solar cell devices with a typical configuration of indium tin oxide (ITO)/Poly(3,4-ethylenedioxythiophene):poly(styrenesulfonate) (PEDOT:PSS)/SMs:PC₇₁BM/Ca/Al was

fabricated as follows: The ITO glass was pre-cleaned with deionized water, acetone and isopropanol in turn for 15 min. The organic residues were further removed by treating with UV-ozone for 1 h. Then the ITO glass was modified by spin-coating PEDOT: PSS (30 nm) on it. After the ITO glasses were dried in oven at 150°C for 15 min, the active layer was spin-coated on the ITO/PEDOT:PSS using a blend solution of SMs:PC₇₁BM (30 mg/mL in o-dichlorobenzene, variants with donor/acceptor weight ratio, and different contents of DIO, respectively). Ca (20 nm) and Al (80 nm) electrode was then subsequently thermally evaporated on the active layer under the vacuum of 1×10^{-4} Torr. The active area of the device was 0.1 cm², and the thicknesses of the active films were recorded by a profilometer (Dektak XT, Bruker). The devices were characterized under the illumination of simulated AM 1.5 G, 100 mW cm⁻² using a solar simulator. The current density-voltage (*J-V*) measurement of the devices was conducted on a computer controlled Keithley 2400 Source Measure Unit. The external quantum efficiency (EQE) measurements were performed in air using a source meter, silicon photodiode, and a computer-controlled light source-monochromator-lock-in system with a scan increment of 20 nm per point.

2.4 Synthesis

2.4.1 Synthesis of compound **4**

To a stirred solution of compound **3** (1.0 g, 2.5 mmol) in methanol (20 mL) and CH₂Cl₂ (20 mL) in a 100 mL three-neck flask were charged ICl (0.49 g, 3.0 mmol) under argon atmosphere for 1 h. The progress of the reaction was monitored by TLC using hexane:CH₂Cl₂ as eluent. After completion of the reaction, the mixture was poured into water and extracted with CH₂Cl₂. The organic layers were separated, dried over Mg₂SO₄, and filtered. Solvents were removed under

reduced pressure and the crude residue was further purified by column chromatography (hexane:CH₂Cl₂ 20:1, v/v) to afford the compound **4** as a red solid (0.78 g, yield: 60%). ¹H NMR (400 MHz, CDCl₃): δ 7.97 (s, 1H), 7.82 (s, 1H), 7.53 (s, 1H), 7.51 (s, 1H), 7.04 (d, *J* = 8.8 Hz, 4H), 6.62–6.58 (m, 1H), 4.06 (t, *J* = 6.5 Hz, 2H), 1.84 (dd, *J* = 14.7, 6.8 Hz, 2H), 1.53–1.29 (m, 10H), 0.90 (t, *J* = 6.9 Hz, 3H). ¹³C NMR (101 MHz, CDCl₃): δ 162.17, 146.82, 145.96, 145.05, 135.94, 135.73, 135.01, 132.93, 132.56, 125.66, 119.34, 114.78, 68.47, 31.86, 29.37, 29.29, 29.17, 26.07, 22.72, 14.17. MALDI-TOF-MS, *m/z*: calcd for C₂₃H₂₆BF₂IN₂O [M]⁺: 522.115; found 522.098.

2.4.2 Synthesis of compound **5**

According to the literature [58], to a mixture of 2,7-dibromo-9H-fluorene (3.24 g, 10 mmol), bromooctane (4 mL, 23 mmol) and tetrabutylammonium bromide (TBAB, catalytic amount) in DMSO (100 mL) was added sodium hydroxide solution (25 mL, 50 wt%). The resulting mixture was stirred at room temperature for 8 h. The progress of the reaction was monitored by TLC using hexane:CH₂Cl₂ as the eluent. After completion of the reaction, the reaction mixture was poured into water and extracted with CH₂Cl₂. The organic layers were separated, dried over anhydrous Mg₂SO₄, and filtered. Solvents were removed under reduced pressure and the crude residue was further purified by column chromatography (hexane as eluent) to afford the compound **5** as a white solid (4.95 g, yield: 91%). ¹H NMR (400 MHz, CDCl₃): δ 7.51 (d, *J* = 8.5 Hz, 2H), 7.47–7.41 (m, 4H), 1.97–1.85 (m, 4H), 1.29–0.97 (m, 20H), 0.83 (t, *J* = 7.1 Hz, 6H), 0.58 (s, 4H). ¹³C NMR (101 MHz, CDCl₃): δ 152.44, 139.19, 130.14, 126.16, 121.46, 121.12, 55.64, 40.25, 31.76, 29.86, 29.18, 29.16, 23.62, 22.60, 14.09.

2.4.3 Synthesis of compound 6

According to the modified literature [57], to the mixture of compound **5** (3.0 g, 5.5 mmol), Pd(PPh₃)₂Cl₂ (0.53 g, 0.55 mmol) and CuI (0.217 g, 1.1 mmol) in Et₃N (50 mL) was added trimethylsilylacetylene (3.1 mL, 22 mmol). The resulting suspension was stirred at 80 °C for 24 h under argon atmosphere. The progress of the reaction was monitored by TLC using hexane:CH₂Cl₂ as the eluent. After cooled to room temperature, the reaction mixture was filtered and the filtrate was evaporated to dryness. The solid obtained was dissolved in CH₂Cl₂, washed with brine, dried with anhydrous Mg₂SO₄ and filtered. Solvents were removed under reduced pressure and the crude residue was further purified by column chromatography (hexane as eluent) to afford the compound **6** as a white solid (2.44 g, yield: 76%). ¹H NMR (400 MHz, CDCl₃): δ 7.59 (d, *J* = 7.8 Hz, 2H), 7.45 (d, *J* = 7.9 Hz, 2H), 7.41 (s, 2H), 1.96–1.89 (m, 4H), 1.24–1.00 (m, 20H), 0.82 (t, *J* = 7.1 Hz, 6H), 0.51 (s, 4H), 0.28 (s, 18H). ¹³C NMR (101 MHz, CDCl₃): δ 150.94, 140.87, 131.24, 126.22, 121.73, 119.86, 106.09, 94.26, 55.24, 40.36, 31.81, 29.99, 29.26, 23.60, 22.62, 14.12, 0.07.

2.4.4 Synthesis of compound 7

To a stirred solution of compound **6** (2.33 g, 4 mmol) in THF (20 mL) was added tetrabutylammonium fluoride (2 mL, 1 mol/L) dropwise. The resulting mixture was further stirred at room temperature for 30 min. After completion of the reaction, the reaction mixture was poured into water and extracted with ethyl acetate. The organic layers were separated, dried over anhydrous Mg₂SO₄, and filtered. Solvents were removed under reduced pressure and the crude residue was further purified by column chromatography (hexane as eluent) to afford the compound

7 as a white solid (1.68 g, yield: 96%). ^1H NMR (400 MHz, CDCl_3): δ 7.63 (d, $J = 7.8$ Hz, 2H), 7.48 (dd, $J = 7.8, 1.3$ Hz, 2H), 7.46 (s, 2H), 3.15 (s, 2H), 1.96–1.90 (m, 4H), 1.22–1.02 (m, 20H), 0.82 (t, $J = 7.1$ Hz, 6H), 0.60–0.53 (m, 4H). ^{13}C NMR (101 MHz, CDCl_3): δ 151.07, 141.00, 131.26, 126.56, 120.85, 119.98, 84.54, 55.23, 40.21, 31.77, 29.94, 29.21, 23.66, 22.59, 14.07. MALDI-TOF-MS, m/z : calcd for $\text{C}_{33}\text{H}_{42}$ $[\text{M}-\text{H}]^+$: 437.329; found 437.235.

2.4.5 Synthesis of compound **8**

Compound **8** was synthesized according to the same procedure as for preparing compound **5** using 2,7-dibromo-9H-carbazole as reactant. The crude product was purified on silica column using hexane as eluent to give the pure compound **8** as a white solid in 92% yield. ^1H NMR (400 MHz, CDCl_3): δ 7.87 (d, $J = 8.3$ Hz, 2H), 7.52 (s, 2H), 7.33 (d, $J = 8.3$ Hz, 2H), 4.17 (t, $J = 7.3$ Hz, 2H), 1.92–1.76 (m, 2H), 1.38–1.21 (m, 10H), 0.87 (t, $J = 6.7$ Hz, 3H). ^{13}C NMR (101 MHz, CDCl_3): δ 141.33, 122.51, 121.47, 121.26, 119.69, 111.99, 43.57, 31.80, 29.31, 29.19, 28.79, 27.19, 22.65, 14.12.

2.4.6 Synthesis of compound **9**

Compound **9** was synthesized according to the same procedure as for preparing compound **6** using compound **8** as reactant. The crude product was purified on silica column using hexane as eluent to give the compound **9** as a white solid in 72% yield. ^1H NMR (400 MHz, CDCl_3): δ 7.96 (d, $J = 8.0$ Hz, 2H), 7.50 (s, 2H), 7.34 (d, $J = 8.0$ Hz, 2H), 4.26–4.21 (m, 2H), 1.85 (dd, $J = 14.1, 7.2$ Hz, 2H), 1.40–1.27 (m, 10H), 0.88 (d, $J = 6.5$ Hz, 3H), 0.31–0.29 (m, 18H). ^{13}C NMR (101 MHz, CDCl_3): δ 140.55, 123.27, 122.67, 120.37, 120.32, 112.42, 106.45, 93.85, 43.20, 31.84, 29.36, 29.21, 28.94, 27.21, 22.64, 14.12.

2.4.7 Synthesis of compound **10**

Compound **10** was synthesized according to the same procedure as for preparing compound **7** using compound **9** as reactant. The crude product was purified on silica column using hexane as eluent to give the compound **10** as a white solid in 95% yield. ^1H NMR (400 MHz, CDCl_3): δ 8.00 (d, $J = 8.0$ Hz, 2H), 7.55 (s, 2H), 7.38–7.35 (m, 2H), 4.24 (t, $J = 7.4$ Hz, 2H), 3.17 (s, 2H), 1.84 (dd, $J = 14.7, 7.3$ Hz, 2H), 1.39–1.24 (m, 10H), 0.87 (t, $J = 6.9$ Hz, 3H). ^{13}C NMR (101 MHz, CDCl_3): δ 140.52, 123.23, 122.83, 120.55, 119.34, 112.76, 84.89, 76.95, 43.25, 31.81, 29.36, 29.20, 28.92, 27.25, 22.64, 14.12. MALDI-TOF-MS, m/z : calcd for $\text{C}_{24}\text{H}_{25}\text{N}$ $[\text{M}]^+$: 327.199; found 327.233.

2.4.8 Synthesis of compound **12**

To a stirred solution of compound **11** (3.0 g, 6.72 mmol) in CH_2Cl_2 (40 mL) was added liquid bromine (2.26 g, 14.12 mmol) dropwise at 0 °C. The resulting mixture was stirred at room temperature for further 7 h. After completion of the reaction, the reaction mixture was poured into water and extracted with ethyl acetate. The organic layers were separated, dried over anhydrous Mg_2SO_4 , and filtered. Solvents were removed under reduced pressure and the crude residue was further purified by column chromatography (hexane as eluent) to afford the compound **12** as a white solid (3.74 g, yield: 92%). ^1H NMR (400 MHz, CDCl_3): δ 7.42 (d, $J = 5.5$ Hz, 2H), 4.15 (t, $J = 6.5$ Hz, 4H), 2.04–1.89 (m, 4H), 1.46–1.22 (m, 20H), 0.90 (t, $J = 6.7$ Hz, 6H). ^{13}C NMR (101 MHz, CDCl_3): δ 142.73, 131.16, 130.90, 123.14, 114.91, 74.17, 31.84, 30.45, 29.38, 29.28, 25.99, 22.69, 14.15.

2.4.9 Synthesis of compound **13**

Compound **13** was synthesized according to the same procedure as for preparing compound **6** using compound **12** as reactant. The crude product was purified on silica column using hexane as eluent to give the compound **13** as yellow oil in 80% yield. ^1H NMR (400 MHz, CDCl_3): δ 7.57 (s, 2H), 4.21 (t, $J = 6.5$ Hz, 4H), 1.92–1.78 (m, 4H), 1.33 (d, $J = 15.4$ Hz, 20H), 0.90 (t, $J = 6.3$ Hz, 6H), 0.28 (s, 18H). ^{13}C NMR (101 MHz, CDCl_3): δ 143.88, 131.80, 130.28, 126.00, 122.89, 101.67, 97.81, 74.17, 31.85, 30.50, 29.41, 29.29, 26.00, 22.71, 14.18.

2.4.10 Synthesis of compound **14**

Compound **14** was synthesized according to the same procedure as for preparing compound **7** using compound **13** as reactant. The crude product was purified on silica column using hexane as eluent to give the compound **14** as yellow oil in 96% yield. ^1H NMR (400 MHz, CDCl_3): δ 7.63 (s, 2H), 4.23 (t, $J = 6.5$ Hz, 4H), 3.48 (s, 2H), 1.88–1.82 (m, 4H), 1.35 (dd, $J = 14.4, 10.3$ Hz, 20H), 0.91 (d, $J = 6.5$ Hz, 6H). ^{13}C NMR (101 MHz, CDCl_3): δ 143.99, 131.72, 130.26, 126.63, 121.93, 83.50, 77.29, 74.26, 31.86, 30.48, 29.41, 29.30, 26.02, 22.71, 14.17. MALDI-TOF-MS, m/z : calcd for $\text{C}_{30}\text{H}_{38}\text{O}_2\text{S}_2$ $[\text{M}]^+$: 494.231; found 494.207.

2.4.11 Synthesis of compound **15**

Compound **15** was synthesized according to the same procedure as for preparing compound **5** using 10H-phenothiazine as reactant. The crude product was purified on silica column using hexane as eluent to give the compound **15** as colorless oil in 92% yield. ^1H NMR (400 MHz, CDCl_3): δ 7.16–7.12 (m, 2H), 7.11 (s, 2H), 6.89 (dd, $J = 8.1, 6.9$ Hz, 2H), 6.84 (d, $J = 7.7$ Hz, 2H), 3.85–3.77 (m, 2H), 1.83–1.73 (m, 2H), 1.36–1.15 (m, 10H), 0.86 (t, $J = 5.9$ Hz, 3H). ^{13}C NMR (101 MHz, CDCl_3): δ 145.38, 127.48, 127.23, 124.93, 122.36, 115.44, 47.46, 31.84, 29.31, 27.05,

26.96, 22.73, 14.22.

2.4.12 Synthesis of compound **16**

Compound **16** was synthesized according to the same procedure as for preparing compound **12** using compound **15** as reactant. The crude product was purified on silica column using hexane as eluent to give the compound **16** as yellow oil in 93% yield. ^1H NMR (400 MHz, CDCl_3): δ 7.26–7.18 (m, 4H), 6.66 (d, $J = 8.5$ Hz, 2H), 3.73 (t, $J = 7.1$ Hz, 2H), 1.80–1.67 (m, 2H), 1.43–1.16 (m, 10H), 0.86 (t, $J = 6.8$ Hz, 3H). ^{13}C NMR (101 MHz, CDCl_3): δ 144.14, 130.13, 129.71, 126.43, 116.67, 114.75, 47.61, 31.76, 29.23, 29.18, 26.83, 26.65, 22.67, 14.17.

2.4.13 Synthesis of compound **17**

Compound **17** was synthesized according to the same procedure as for preparing compound **6** using compound **16** as reactant. The crude product was purified on silica column using hexane as eluent to give the compound **17** as yellow oil in 70% yield. ^1H NMR (400 MHz, CDCl_3): δ 7.22 (dd, $J = 8.4, 1.9$ Hz, 2H), 7.18 (d, $J = 1.9$ Hz, 2H), 6.71 (d, $J = 8.5$ Hz, 2H), 3.81–3.75 (m, 2H), 1.79–1.69 (m, 2H), 1.39–1.22 (m, 10H), 0.87 (t, $J = 6.8$ Hz, 3H), 0.23 (s, 18H). ^{13}C NMR (101 MHz, CDCl_3): δ 144.73, 131.19, 130.59, 123.97, 117.21, 114.97, 104.33, 94.03, 47.66, 31.74, 29.20, 29.15, 26.76, 26.62, 22.64, 14.12.

2.4.14 Synthesis of compound **18**

Compound **18** was synthesized according to the same procedure as for preparing compound **7** using compound **17** as reactant. The crude product was purified on silica column using hexane as eluent to give the compound **18** as yellow oil in 94% yield. ^1H NMR (400 MHz, CDCl_3): δ 7.28–7.24 (m, 2H), 7.20 (d, $J = 1.7$ Hz, 2H), 6.75 (d, $J = 8.4$ Hz, 2H), 3.82–3.77 (m, 2H), 3.04 (s,

2H), 1.79–1.72 (m, 2H), 1.26 (dd, $J = 11.8, 5.5$ Hz, 10H), 0.86 (t, $J = 6.7$ Hz, 3H). ^{13}C NMR (101 MHz, CDCl_3): δ 145.04, 131.45, 130.75, 124.10, 116.27, 115.11, 82.90, 77.14, 47.68, 31.73, 29.19, 29.15, 26.80, 26.66, 22.63, 14.11. MALDI-TOF-MS, m/z : calcd for $\text{C}_{24}\text{H}_{25}\text{NS}$ $[\text{M}]^+$: 359.171; found 359.186.

2.4.15 Synthesis of compound **F-BDP**

According to the modified procedure [57], compound **4** (131 mg, 0.25 mmol), $\text{Pd}(\text{PPh}_3)_2\text{Cl}_2$ (7 mg, 0.01 mmol) and CuI (2.0 mg, 0.01 mmol) were dissolved in dry toluene (10 mL) and Et_3N (10 mL) under nitrogen. Degassed compound **7** (44 mg, 0.1 mmol) in toluene (5 mL) solution was added. After purging with nitrogen for 15 min, the mixture was stirred at room temperature for 12 h under nitrogen. After completion of the reaction, the reaction mixture was poured into water and extracted with ethyl acetate. The organic layers were separated, dried over anhydrous Mg_2SO_4 , and filtered. Solvents were removed under reduced pressure and the crude residue was further purified by column chromatography (ethyl acetate/hexane 1:5, v/v) to give the desired **F-BDP** as black purple solid (88 mg, yield: 72%). ^1H NMR (400 MHz, CDCl_3): δ 8.06 (s, 2H), 7.98 (s, 2H), 7.64 (d, $J = 7.6$ Hz, 2H), 7.57 (s, 2H), 7.55 (s, 2H), 7.48–7.43 (m, 4H), 7.10 (s, 2H), 7.05 (d, $J = 8.6$ Hz, 6H), 6.62–6.58 (m, 2H), 4.06 (t, $J = 6.5$ Hz, 4H), 1.97–1.93 (m, 4H), 1.89–1.82 (m, 4H), 1.37–1.03 (m, 40H), 0.90 (t, $J = 6.8$ Hz, 6H), 0.82 (d, $J = 6.8$ Hz, 6H), 0.59 (s, 4H). ^{13}C NMR (101 MHz, CDCl_3): δ 162.08, 151.32, 151.14, 147.54, 144.78, 140.69, 135.48, 134.17, 132.58, 132.37, 131.58, 130.55, 126.95, 125.81, 121.77, 120.23, 120.01, 119.07, 114.71, 92.85, 82.73, 68.45, 55.23, 40.33, 31.84, 31.79, 30.01, 29.99, 29.35, 29.26, 29.25, 29.16, 26.05, 23.73, 22.65, 22.69, 14.13, 14.09. MALDI-TOF-MS, m/z : calcd for $\text{C}_{79}\text{H}_{92}\text{B}_2\text{F}_4\text{N}_4\text{O}_2$ $[\text{M}]^+$: 1226.734; found 1226.352. HRMS, m/z : calcd for $\text{C}_{79}\text{H}_{92}\text{B}_2\text{F}_4\text{N}_4\text{O}_2$ $[\text{M}]^+$: 1226.7343; found 1226.7340.

2.4.16 Synthesis of compound **C-BDP**

Compound **C-BDP** was synthesized according to the same procedure as for preparing compound **F-BDP** using compound **4** and compound **10** as reactants. The crude product was purified on silica column using hexane as eluent to give the desired compound **C-BDP** as black purple solid in 68% yield. ^1H NMR (400 MHz, CDCl_3): δ 8.08 (s, 2H), 8.02–7.97 (m, 4H), 7.58 (d, $J = 1.9$ Hz, 2H), 7.57–7.55 (m, 2H), 7.52 (s, 2H), 7.34 (dd, $J = 8.1, 1.2$ Hz, 2H), 7.12 (s, 2H), 7.08–7.04 (m, 6H), 6.60 (dd, $J = 4.3, 1.8$ Hz, 2H), 4.26 (t, $J = 7.3$ Hz, 2H), 4.07 (t, $J = 6.5$ Hz, 4H), 1.86 (dd, $J = 14.2, 7.2$ Hz, 6H), 1.41–1.24 (m, 30H), 0.92–0.85 (m, 9H). ^{13}C NMR (101 MHz, CDCl_3): δ 162.08, 147.53, 144.88, 144.72, 140.72, 135.48, 134.19, 132.59, 132.34, 131.59, 125.83, 122.72, 122.58, 120.52, 120.30, 119.15, 114.71, 114.20, 111.85, 93.22, 82.29, 68.45, 43.30, 31.84, 29.39, 29.36, 29.27, 29.21, 29.16, 28.97, 27.31, 26.06, 22.69, 22.63, 14.14, 14.10. MALDI-TOF-MS, m/z : calcd for $\text{C}_{70}\text{H}_{75}\text{B}_2\text{F}_4\text{N}_5\text{O}_2$ $[\text{M}]^+$: 1115.604; found 1115.271. HRMS, m/z : calcd for $\text{C}_{70}\text{H}_{75}\text{B}_2\text{F}_4\text{N}_5\text{O}_2$ $[\text{M}]^+$: 1115.6043; found 1115.6035.

2.4.17 Synthesis of compound **B-BDP**

Compound **B-BDP** was synthesized according to the same procedure as for preparing compound **F-BDP** using compound **4** and compound **14** as reactants. The crude product was purified on silica column using hexane as eluent to give the desired compound **B-BDP** as black purple solid in 58% yield. ^1H NMR (400 MHz, CDCl_3): δ 8.04 (s, 2H), 8.00 (s, 2H), 7.56 (d, $J = 7.1$ Hz, 6H), 7.07 (dd, $J = 10.8, 7.9$ Hz, 8H), 6.61 (d, $J = 2.5$ Hz, 2H), 4.24 (t, $J = 6.5$ Hz, 4H), 4.07 (t, $J = 6.5$ Hz, 4H), 1.85 (dd, $J = 13.3, 6.6$ Hz, 8H), 1.33 (d, $J = 18.3$ Hz, 40H), 0.92–0.88 (m, 12H). ^{13}C NMR (101 MHz, CDCl_3): δ 162.19, 147.87, 145.62, 145.36, 144.36, 143.83, 135.68,

134.09, 132.83, 132.61, 131.94, 131.54, 130.34, 125.70, 125.11, 122.89, 119.38, 114.77, 88.67, 85.46, 74.17, 68.47, 53.43, 31.85, 31.83, 30.52, 29.71, 29.41, 29.35, 29.26, 29.15, 26.04, 26.03, 22.68, 14.13. MALDI-TOF-MS, m/z: calcd for $C_{76}H_{88}B_2F_4N_4O_4S_2$ $[M]^+$: 1282.637; found 1282.170. HRMS, m/z: calcd for $C_{76}H_{88}B_2F_4N_4O_4S_2$ $[M]^+$: 1282.6369; found 1282.6358.

2.4.18 Synthesis of compound **P-BDP**

Compound **P-BDP** was synthesized according to the same procedure as for preparing compound **F-BDP** using compound **4** and compound **18** as reactants. The crude product was purified on silica column using hexane as eluent to give the desired compound **P-BDP** as black purple solid in 61% yield. 1H NMR (400 MHz, $CDCl_3$): δ 7.99 (s, 2H), 7.95 (s, 2H), 7.55 (s, 2H), 7.53 (s, 2H), 7.23 (dd, $J = 8.4, 1.9$ Hz, 2H), 7.18 (d, $J = 1.9$ Hz, 2H), 7.04 (d, $J = 8.6$ Hz, 8H), 6.76 (d, $J = 8.5$ Hz, 2H), 6.58 (dd, $J = 4.2, 1.7$ Hz, 2H), 4.06 (t, $J = 6.5$ Hz, 4H), 3.81 (t, $J = 7.2$ Hz, 2H), 1.88–1.75 (m, 6H), 1.42–1.23 (m, 30H), 0.89 (dd, $J = 14.0, 6.9$ Hz, 9H). ^{13}C NMR (101 MHz, $CDCl_3$): δ 162.06, 147.48, 144.82, 144.60, 135.42, 134.14, 132.55, 132.24, 131.46, 130.72, 129.97, 125.82, 124.11, 118.93, 117.23, 115.16, 114.70, 91.12, 82.33, 77.74, 77.09, 76.78, 68.44, 47.74, 31.83, 31.73, 29.34, 29.26, 29.18, 9.15, 26.82, 26.72, 26.04, 22.68, 22.62, 14.11, 14.09. MALDI-TOF-MS, m/z: calcd for $C_{70}H_{75}B_2F_4N_5O_2S$ $[M]^+$: 1147.576; found 1147.256. HRMS, m/z: calcd for $C_{70}H_{75}B_2F_4N_5O_2S$ $[M]^+$: 1147.5764; found 1147.5760.

3. Results and discussion

3.1 Synthesis and characterization

The synthetic routes for the novel A-D-A type β -alkynylated BODIPY derivatives, **F-BDP**, **C-BDP**, **B-BDP** and **P-BDP** are depicted in Scheme 1. For the construction of these molecules, we utilized the Pd-catalyzed Sonogashira reaction to connect two BODIPY units covalently to the

central electron-donating unit with alkynyl bridges, where β -iodinated BODIPY **4** and bisalkynyl substituted donor moiety should be prerequisite for the synthesis. Firstly, iodination of BODIPY **3** with 1.3 equiv of ICl in the mixture solvent of methanol and methylene chloride readily afford the β -iodinated BODIPY **4** with a moderate yield. Secondly, treatment of bisbrominated alkyl donors **5**, **8**, **12**, **16**, with trimethylsilylacetylene in the presence of catalytic amount of Pd(PPh₃)₂Cl₂ and CuI in Et₃N, following by charging with tetrabutylammonium fluoride smoothly give the desired bisalkynyl substituted donors **7**, **10**, **14**, **18**. With these key intermediates in hand, finally, the target molecules **F-BDP**, **C-BDP**, **B-BDP** and **P-BDP**, were achieved by the Pd-catalyzed Sonogashira coupling of β -iodinated BODIPY **4** with the corresponding electron donors. These newly synthesized target molecules were sufficiently soluble in THF, CHCl₃, CH₂Cl₂, o-dichlorobenzene to permit their characterization in solution as well as their application in BHJ-OSCs devices. The structure assignments of these novel molecules were confirmed by NMR spectroscopy, MALDI-TOF-MS and HRMS.

3.2 Thermal properties

The thermal properties of four SMs are evaluated with TGA and DSC. The recorded TGA and DSC curves are depicted in Fig. 1 and Fig. S1 (ESI), respectively. The corresponding data are summarized in Table 1. As displayed, all of four SMs shown high thermal stability with the decomposition temperatures (T_d , at 5% weight loss) observed at 314 °C, 300 °C, 295 °C and 301 °C for **F-BDP**, **C-BDP**, **B-BDP** and **P-BDP**, respectively, which is good enough for the OSCs application. It indicates that the different electron donors have significant effect on their thermal properties. Fluorene-based **F-BDP** has higher thermal stability than carbazole- and phenothiazine-based **C-BDP** and **P-BDP**, and BDT based **B-BDP** exhibits the relatively lower T_d value. In DSC, the dyes were heated from 25 to 300 °C and then again cooled to 25 °C with a rate of 10 °C/min under nitrogen flow. As shown in Fig S1, **F-BDP** exhibits an endothermic peak at 187 °C, which indicates the melting temperature of **F-BDP**. Nevertheless, no exothermic peak is observed during

the cooling process in DSC curve. Similarly, **C-BDP**, **B-BDP** and **P-BDP** display endothermic peaks at 191 °C, 184 °C and 169 °C, respectively. The results show that all of these SMs have high thermal stability and good enough for the application in optoelectronic devices.

3.3 Absorption spectra

The UV-vis absorption spectra of reference BODIPY **3**, **F-BDP**, **C-BDP**, **B-BDP** and **P-BDP** are shown in Fig. 2, and their corresponding optical data are summarized in Table 1. As shown, both SMs exhibited the similar absorption spectra covering from 300 to 650 nm with two obvious absorption peaks, in which the high-lying region from 300 to 450 nm originate from the localized π - π^* transition of the conjugated backbones, whereas the low-lying region from 470 to 650 nm is assigned to the S_0 - S_1 transition along with the ICT interaction between central donor moiety and terminal BODIPY acceptor moieties. In comparison with the reference BODIPY **3**, SMs all showed obviously broad and red-shifted (~ 50 nm) absorption spectra. It indicated that the conjugate length was effectively extended by flanking two BODIPY units on the central donor unit though acetylene bridges, leading to an intense ICT, and therefore, resulting a narrow band gap. The optical band gaps calculated from the absorption onset wavelength (λ_{onset}) were 1.89 eV for **F-BDP**, 1.87 eV for **C-BDP**, 1.84 eV for **B-BDP** and 1.79 for **P-BDP**, according to the formula of $E_g^{\text{opt}} = 1240/\lambda_{\text{onset}}$. The molecular extinction coefficients (ϵ) of BODIPY **3**, **F-BDP**, **C-BDP**, **B-BDP** and **P-BDP** are 5.9×10^4 , 4.8×10^4 , 8.2×10^4 , 8.4×10^4 , 3.7×10^4 and 4.7×10^4 $\text{cm}^{-1} \text{M}^{-1}$, respectively (Table 1). Such high molecular extinction coefficients enable these SMs for good light-harvesting ability. As displayed, **F-BDP** and **C-BDP** exhibit higher ϵ value than the typical BODIPY, is mainly attributed to the intense ICT between the strong electron-donating fluorene and carbazole segment and the electron-accepting BODIPY dye units. On the other hand,

B-BDP and **P-BDP** display relatively lower ϵ value than that of **F-BDP** and **C-BDP**, suggesting that the central electron donating motif can easily tune the molecular extinction coefficients.

In comparison with the absorption spectrum in solution, broader absorption bands with significant bathochromic shifts were observed in thin film (Fig. 3) for these SMs. This could be attributed to the molecular aggregation and interchain interactions in the solid state, which resulting an additional increasement of conjugation length. It is worth noting that **B-BDP** exhibits a much more obviously bathochromic shifts than other SMs. It is due to the fact that **B-BDP** has the ability to form short non-covalent S...S contact with adjacent molecules [59], leading to better intermolecular interactions and further extended the conjugation length. Broad and intense absorption properties of these SMs make them good candidates for the light-harvesting and photovoltaic applications.

3.4 Emission spectra

The photoluminescence (PL) of **F-BDP**, **C-BDP**, **B-BDP** and **P-BDP** in CH_2Cl_2 solution (1×10^{-7} mol/L) were investigated at room temperature. Rhodamine B (= 0.71) was used as standard in methanol to estimate the fluorescence quantum yield. All the SMs were excited by the λ_{max} of their absorption spectra and the normalized emission spectra are illustrated in Fig. 4, and the emission band maxima, Stokes shift and quantum yields are listed in Table 1, respectively. Unlike to the ever reported that the BODIPY derivatives are usually with small Stokes shifts, these SMs exhibit obvious Stokes shifts (55-89 nm), resulting in maximum emission peak at 632, 643, 624 and 603 nm, respectively (Table 1 and Fig. 4). This can be explained on the basis of intramolecular energy transfer from the BODIPY $\pi\text{-}\pi^*$ excited state to the lower lying singlet excited state of the donor moieties and/or to the existence of new non-radiative pathways from the BODIPY $\pi\text{-}\pi^*$ excited

state to the ground state. In general, the strong donor-acceptor interaction and coplanar molecular configuration will decrease the excitation energy of the excited state and will shift the fluorescence emission band to the long wavelength region. Accordingly, as shown in Fig. 4, **F-BDP** and **C-BDP**, incorporating donor units with strong electron-donating capacity, display more significant Stokes shifts. On the other hand, **F-BDP**, **C-BDP**, **B-BDP** and **P-BDP** all give low fluorescent quantum yields (0.02-0.05). These could be attributed to the increased internal conversion according to the energy gap law that states the non-radiative deactivation probability of S_0 - S_1 increases as the energy gap of S_0 - S_1 decreases in an extended conjugating system. PL quenching provides the direct evidence for excitation dissociation, and efficient PL quenching is necessary to obtain efficient organic solar cells. The experimental observations indicate that these SMs are well meet requirements of material for OSCs.

3.5 Electrochemical properties

To investigate the electrochemical behaviors of **F-BDP**, **C-BDP**, **B-BDP** and **P-BDP**, their electronic states were studied by cyclic voltammetry (CV) in CH_2Cl_2 solution containing 0.1M Bu_4NPF_6 at a scan rate of 100 mV s^{-1} , and the cyclic voltammograms were calibrated with ferrocene/ferrocenium (Fc/Fc^+) as an external reference. The CV curves were depicted in Fig. 5 and the results are summarized in Table 2. As shown in Fig. 5, **F-BDP**, **C-BDP**, **B-BDP** and **P-BDP** present differential first onset oxidation potential as 0.96, 0.90, 0.83 and 0.74 V, respectively, indicating the central donor have significant effects on the $E_{\text{onset}}^{\text{ox}}$. The reduction potentials (E_{red}) calculated from $E_{\text{onset}}^{\text{ox}} - E_{\text{g}}^{\text{opt}}$ are approximately matched with the experimental values obtained from reduction waves. The HOMO and LUMO levels were estimated using the equation:

$$E_{\text{HOMO}} = [-(E_{\text{onset}}^{\text{ox}} - 0.52) - 4.8] \text{ eV}, \quad E_{\text{LUMO}} = E_{\text{HOMO}} + E_{\text{g}}^{\text{opt}} \text{ eV}$$

where 0.52 V is the value for ferrocene vs Ag/AgCl and 4.8 eV is the energy level of Fc/Fc⁺ relative to the vacuum energy level. The calculated HOMO energy levels of these SMs are obtained as -5.24 eV for **F-BDP**, -5.18 eV for **C-BDP**, -5.11 eV for **B-BDP** and -5.02 eV for **P-BDP**, respectively, as list in Table 2. On the contrary, the LUMO values are observed with minor difference for the SMs, suggesting that the reduction of the BODIPY moiety within the molecule is relatively immune to the core donor moiety. Their low-lying HOMO energy levels suggest that the OSCs based on these materials as donors and PCBM as acceptor can obtain high V_{oc} .

3.6 Theoretical calculations

To better understand the variation in photophysical and electrochemical properties between **F-BDP**, **C-BDP**, **B-BDP** and **P-BDP**, the density functional theory (DFT) theoretical calculation was conducted on the electronic structures of them to observe how they impact these properties. The optimized ground-state geometries and electronic distribution in HOMO-LUMO levels were presented in Fig. 6. All the calculations were carried out with the Gaussian 09 program suite by using the B3LYP method and 6-31 G* basis set. In the optimized ground-state, we observed that the dihedral angle between the central donor motif and flanked BODIPY are calculated to be 0.7° for **F-BDP**, 11.6° for **C-BDP**, 11.0° for **B-BDP** and 19.1° for **P-BDP**, respectively. In comparison to those similar molecules without ethynyl bridges reported in the previous literature [50], the ethynyl linked SMs show much more planar molecular geometry. For example, BDP3, with two fluorene groups directly substituted at the 2,6-positions of BODIPY, display dihedral angle of 25.7° between the fluorene group and the central BODIPY core. In contrast, **F-BDP**, with ethynyl

bridges between the fluorene group and BODIPY present in this paper, exhibit significant smaller value of 0.7° . Similarly result was observed that **C-BDP** also show smaller dihedral angles than BDP4 (11.6° vs 22.8°). These comparative results demonstrated that the ethynyl bridge play an important role in optimization of molecular configuration. A near-planar molecular configuration in D-A conjugate can efficiently arouse intense ICT, resulting in decrease of band gap and red shifted absorption, which was clearly observed in absorption spectra. Furthermore, planar molecular structure facilitate for hole mobility and energy transfer, which are considered as key factors for high-performance photovoltaic devices. The efficient energy transfer from BODIPY units to the donor unit in the excited state has been verified by the PL spectra with large Stokes shift and low fluorescence quantum yield. From the electron distributions of **F-BDP** and **C-BDP**, it can be seen that π - electrons in the HOMOs are delocalized over the entire molecule backbone, offering effective orbital interactions among the stacked π -systems, while their LUMOs are mainly localized on the BODIPY moieties, indicating that the HOMO-LUMO transition that is the dominant contributing configuration to the S_1 state in **F-BDP** and **C-BDP** should be ascribed to a mixture of π - π^* and ICT characters. Moreover, the feature of widely spread HOMOs enable to lead to lower HOMO level (-5.3 eV), as observed in Fig. 6. However, for **B-BDP** and **P-BDP**, the HOMOs are centered in donor moiety with some antibonding character between the donor unit and the acceptor unit, and the LUMOs are located in the two BODIPY moieties, indicating that the HOMO-LUMO transition in **B-BDP** and **P-BDP** should mainly be ascribed to the ICT. Fig. 6 also presented the HOMO-LUMO energy levels and energy differences of these SMs. The calculated values of HOMO levels are -5.32 eV for **F-BDP**, -5.31 eV for **C-BDP**, -5.16 eV for **B-BDP**, and -5.05 eV for **P-BDP**, respectively, while the values of LUMO levels are -3.13 eV for **F-BDP**,

-3.13 eV for **C-BDP**, -3.17 eV for **B-BDP**, and -3.07 eV for **P-BDP**, respectively, which are approximately in accordance with the trends of the experimental observation in CV. In addition, the trend of the predicted E_g^{cal} values is in consistent with the estimated E_g^{opt} calculated from the ground-state absorption. The relatively narrow band gap and low-lying HOMO energy levels make them excellent donor materials for OSCs.

3.7 Photovoltaic properties

The solution processed bulk hetero-junction organic solar cells were fabricated with a structure of ITO/PEDOT:PSS/active layer/Ca/Al, in which **F-BDP**, **C-BDP**, **B-BDP** or **P-BDP** was used as the donor material and PC₇₁BM as the acceptor material. With careful optimization of the processing parameters such as the ratio of donor to acceptor (D:A, w/w), the thickness of active layer, the volume of additives and the annealing temperature (Figs. S2–S6, Tables S1–S5, Supporting Information), their best performances were obtained with a 1:1 ratio of donor to PC₇₁BM acceptor and the thicknesses of 100, 80, 80 and 90 nm, associate with thermal annealing at 120, 100, 80 and 100 °C for 10 min obtained from an CB solution at a total solid concentration of 25 mg mL⁻¹ under a spin-coating rate of 2000 rpm, for **F-BDP**, **C-BDP**, **B-BDP** and **P-BDP**, respectively, in the presence of 1% 1,8-diiodooctane (DIO) additive. Fig. 7 shows the current density–voltage (J – V) characteristics of **F-BDP**, **C-BDP**, **B-BDP** and **P-BDP** based BHJ-OSCs under illumination of AM 1.5G 100 mW m⁻² and their corresponding data are listed in Table 3. It is further found that **B-BDP** based device exhibit the highest PCE of 4.65% with a J_{sc} of 11.84 mA cm⁻², a V_{oc} of 0.73 V and a FF of 53.8% in the optimized conditions, which are good values among the BODIPY derivatives based SM-OSCs. Comparative studies show that the **B-BDP** and **P-BDP** (3.33%) based devices have higher PCE values than the **F-BDP** (2.60%) and **C-BDP**

(3.02%) based devices (Fig. 7, Table 3). This is due to the fact that **B-BDP** and **P-BDP** based devices present the higher J_{sc} and FF values, originated from their superior photon-electron conversion and carrier transmission properties in the OSCs. It should be note that **P-BDP** displayed a higher PCE than the ever reported phenothiazine based OSCs [60-61], though the samples are rather scarce. To our pleasant surprise, the BHJ-OSCs based on these β -alkynylated BODIPYs exhibit significant enhancements in device parameters in comparison with the BHJ-OSCs based on β position directly substituted analogues reported in previous works [50], implying that the alkynyl play a important role in the improvement of photovoltaic performances, especially for the J_{sc} through efficient strengthening of light-harvesting, exciton diffusion, exciton dissociation, charge transport, and/or collection process in cells via adjustment of the molecular coplanar. On the other hand, **F-BDP**, **C-BDP** and **B-BDP** based cells show the larger V_{oc} values than **P-BDP** based cell, which is in agreement with their deeper lying HOMO levels. To be note that these BHJ-OSCs all exhibit decent FF (~50%) compared to other BODIPY derivatives analogues. This may be caused by the appropriate length of alkyl chain attachment on the backbone ensure the appropriate crystalline and enable to form good microstructure between the donor and PC₇₁BM.

To further illustrate the differences of photovoltaic performance between these **F-BDP**, **C-BDP**, **B-BDP** and **P-BDP**/PC₇₁BM based OSCs devices, external quantum efficiencies (EQEs) of these devices under optimization condition were measured. The recorded EQE curves are shown in Fig. 8. As displayed, the EQE profiles are similar with their absorption spectra in film. A broad response to the sunlight in 300-800 nm region with different EQEs values are observed for four SMs:PC₇₁BM based OSCs. Higher EQE values of 50% and 40% are exhibited in the **B-BDP** and

P-BDP based devices, respectively. The calculated J_{sc} values are 6.46, 8.01, 11.27 and 9.22 mA cm^{-2} for **F-BDP**, **C-BDP**, **B-BDP** and **P-BDP/PC₇₁BM** blends respectively given by integrated EQE curves, which are in close agreement with the J_{sc} values obtained from the J - V measurements. It is further found that **B-BDP** and **P-BDP/PC₇₁BM** blends based devices exhibit stronger absorption in the 600-700 nm regions than **F-BDP** and **C-BDP/PC₇₁BM** blends based ones, especially cell based on **B-BDP** spread the absorption to 800 nm, which caused the higher EQE values. This is due to the fact that although the sunlight energy in the longer wavelength region is weak, however, the electronic transitions are capable of transformation with sufficient efficiency of photons to electrons, which can be theoretical supported by the electronic distribution characteristic in HOMO-LUMO levels (Fig. 6).

3.8 Hole mobility

In addition to the optical absorption and energy levels, the charge carrier mobility of donor material is another important factor to ensure efficient charge transport toward the electrodes and also to suppress the competing charge recombination processes. In order to get some ideas about the influence of the chemical structures on their charge transporting properties, we evaluated and compared the hole mobilities (μ_h) of **F-BDP**, **C-BDP**, **B-BDP** and **P-BDP** in the same BHJ blends using a space charge-limited current (SCLC) technique. Fig. 9 showed the $J^{1/2}$ - V curves of the vertical hole-only devices with structures of ITO/PEDOT:PSS/SMs:PC₇₁BM/Au. The hole mobilities were determined by fitting the dark $J^{1/2}$ - V characteristics by adopting the Mott-Gurney equation [62]: $J = (9/8)\epsilon_0\epsilon_r\mu_h(V^2/L^3)$, in which J is current density, L is film thickness of active layer (80 nm), μ_h is hole mobility, ϵ_r is relative dielectric constant of the transport medium, ϵ_0 is permittivity of free space (8.85×10^{-12} F m^{-1}), V is internal voltage in the device and $V = V_{appl} - V_a$

$-V_{bi}$, where V_{appl} is applied voltage, V_a is voltage drop, and V_{bi} is the built-in voltage due to the relative work function difference of the two electrodes. As compiled in Table 3, the hole-only mobilities of these SMs are calculated to be $9.61 \times 10^{-5} \text{ cm}^2 \text{ V}^{-1} \text{ s}^{-1}$, $1.34 \times 10^{-4} \text{ cm}^2 \text{ V}^{-1} \text{ s}^{-1}$, $4.53 \times 10^{-4} \text{ cm}^2 \text{ V}^{-1} \text{ s}^{-1}$ and $3.11 \times 10^{-4} \text{ cm}^2 \text{ V}^{-1} \text{ s}^{-1}$ in the hole-only SMs/PC₇₁BM based devices, respectively. It clearly demonstrated that **B-BDP** and **P-BDP** based devices present higher hole-only mobilities than **F-BDP** and **C-BDP** based counterparts, which are in agreement with the *FF* values obtained from the *J-V* measurements.

3.9 Film morphology

The morphologies of the SMs/PC₇₁BM blend films under the optimized processing conditions were recorded with transmission electron microscopy (TEM) and shown in Fig. 10. The observed dark phases are assigned to the PC₇₁BM domains because of its relatively higher electron scattering density. As can be seen, **F-BDP/PC₇₁BM** and **C-BDP/PC₇₁BM** blend films exhibit large black phases with a width around 70-30 nm, On the contrary, the images from **B-BDP/PC₇₁BM** and **P-BDP/PC₇₁BM** blend films present improved morphology with a continuous acicular fibrous structure and a decreased size of around 16 nm. It implying that the continuously interpenetrated networks are formed in **B-BDP** and **P-BDP** based blend films. In general, good morphology would lead to high exciton dissociation and charge separation efficiency and thus enhance device performance. These results are in good agreement with the hole-mobility and photovoltaic observations.

3.10 XRD

To further understand the aggregation behavior of the molecule in film, as well as reveal its

influence on the photoelectric properties and photovoltaic performance, the XRD pattern of **B-BDP**, with the best PCE, was recorded in the pure film and in the blend film with PC₇₁BM under the optimized conditions. As shown in Fig. 11, a sharp peak was observed in the small angle regions with $2\theta = 5^\circ$, corresponding to the interchain d-spacing of 17.66 Å. It indicates that **B-BDP** pack close in thin film. Moreover, a broad peak in the wider angle with $2\theta = 20\text{-}25^\circ$ was also observed, which is attributed to the interlayer π - π staking of the main chain. To get some idea of the change in crystallinity of the blended active layer, we have further recorded the XRD pattern of **B-BDP**/PC₇₁BM blend film under the optimized device conditions. As can be seen, the intensity of the diffraction peak at $2\theta = 5^\circ$ was significant increased under the DIO and annealing treatments as compared with the **B-BDP** film, implying the enhancement in the crystalline nature of the blend. Meanwhile, the π - π staking characteristic peak was obviously decreased. It can be explained as a certain phase separation between the **B-BDP** and PC₇₁BM inhibits the over-aggregation of the donors, which are demonstrated in the TEM observations. The crystallinity of the active layer is one of key factor, which affect the charge transport and light harvesting efficiency of the device, thereby impact the device performance of the OSCs. These results are in agreement with the relatively high hole mobility and EQE, which are reasonable for the high *FF* and *J_{sc}* in OSC.

4. Conclusions

In summary, four linear A-D-A type small molecules with BODIPY terminal linked through alkynyl with various electron donating units, **F-BDP**, **C-BDP**, **B-BDP** and **P-BDP** were designed and synthesized. The molecules show good thermal stability, strong spectral coverage with moderate HOMO energy levels. The influence of alkynyl bridges and the central electron donor

on optical, electrochemical and photovoltaic properties was systematically investigated. As anticipated, the alkynyl group effectively makes electron donor and receptor cell of these molecules in coplanar configurations, resulting in broad absorption, efficient exciton dissociation and good aggregation morphology. All these SMs/PC₇₁BM based OSCs displayed moderate photovoltaic performance with PCE ranging from 2.60% to 4.65%. Among them, **B-BDP** exhibited superior intermolecular interaction in film, leading to enhanced light absorption, as well as increased hole mobility and promoted surface morphology. Consequently, an encouraging PCE value up to 4.65% with a J_{sc} of 11.84 mA cm⁻², a V_{oc} of 0.73 V and a FF of 53.8% was obtained for the **B-BDP/PC₇₁BM** based cell, which is high level in BODIPY based OSCs. This work demonstrates that BODIPY derivatives remain a type of promising photovoltaic material as long as elaborately tailored.

Acknowledgements

We greatly acknowledge the financial support from Nature Science Foundation of Guangdong Province (2016A030313131, 2016A030313128, 2014A030313630), China Postdoctoral Science Foundation (2017M612656), Young Innovative Talents Program of Guangdong Colleges and Universities (2016KQNCX164) and National Nature Science Foundation of China (51476036, 21342003).

Appendix A. Supplementary data

Supplementary data related to this article can be found at

Reference

- [1] Yu G, Gao J, Hummelen JC, Wudl F, Heeger AJ. Polymer photovoltaic cells: enhanced efficiencies via a network of internal donor-acceptor heterojunctions. *Science* 1995;270:1789–91.
- [2] Thompson BC, Fréchet JMJ. Polymer–fullerene composite solar cells. *Angew Chem Int Ed* 2008;47:58–77.
- [3] Cheng YJ, Yang SH, Hsu CS. Synthesis of conjugated polymers for organic solar cell applications. *Chem Rev* 2009;109:5868–923.
- [4] Li G, Zhu R, Yang Y. Polymer solar cells. *Nat Photonics* 2012;6:153–61.
- [5] Dou L, You J, Hong Z, Xu Z, Li G, Street RA, et al. 25th Anniversary article: a decade of organic/polymeric photovoltaic research. *Adv Mater* 2013;25:6642–71.
- [6] He ZC, Xiao B, Wu HB, Cao Y, Russell TP, Wang C, et al. Single-junction polymer solar cells with high efficiency and photovoltage. *Nat Photon* 2015;9:174–9.
- [7] Vohra V, Kawashima K, Kakara T, Murata H, Osaka I, Koganezawa T, et al. Efficient inverted polymer solar cells employing favourable molecular orientation. *Nat Photon* 2015;9:403.
- [8] Liu C, Yi C, Wang K, Gong X, Yang YL, Bhatta SR, et al. Single-junction polymer solar cells with over 10% efficiency by a novel two-dimensional donor-acceptor conjugated copolymer. *ACS Appl Mater Interfaces* 2015;7:4928–35.
- [9] Chen J-D, Cui C, Li Y-Q, Zhou L, Ou Q-D, Li C, et al. Single-junction polymer solar cells exceeding 10% power conversion efficiency. *Adv Mater* 2015;27:1035–41.
- [10] Sun K, Xiao ZY, Lu SR, Jones JD, Pisula W, Williamson RM, et al. A molecular nematic liquid crystalline material for high-performance organic photovoltaics. *Nat Commun* 2015;6:1–9.

- [11] Kan B, Li MM, Zhang Q, Cao Y, Liu F, Chen YF, et al. A series of simple oligomerlike small molecules based on oligothiophenes for solution-processed solar cells with high efficiency. *J Am Chem Soc* 2015;137:3886–93.
- [12] Walker B, Kim C, Nguyen T-Q. Small molecule solution-processed bulk heterojunction solar cells. *Chem Mater* 2011;23:470–82.
- [13] Roncali J, Leriche P, Blanchard P. Molecular materials for organic photovoltaics: small is beautiful. *Adv Mater* 2014;26:3821–38.
- [14] Nielsen CB, Ashraf RS, Schroeder BC, D'Angelo P, Watkins SE, Song K, et al. Random benzotrithiophene-based donor-acceptor copolymers for efficient organic photovoltaic devices. *Chem Commun* 2012;48:5832–4.
- [15] Wong WWH, Subbiah J, Puniredd SR, Pisula W, Jones DJ, Holmes AB. Benzotriazole-based donoreceptor conjugated polymers with a broad absorption in the visible range. *Polym Chem* 2014;5:1258–63.
- [16] Huang Y, Zhang M, Chen H, Wu F, Cao Z, Zhang L, et al. Efficient polymer solar cells based on terpolymers with a broad absorption range of 300-900 nm. *J Mater Chem A* 2014;2:5218–23.
- [17] Carsten B, Szarko JM, Son HJ, Wang W, Lu L, He F, et al. Examining the effect of the dipole moment on charge separation in donoreceptor polymers for organic photovoltaic applications. *J Am Chem Soc* 2011;133:20468–75.
- [18] Carsten B, Szarko JM, Lu L, Son HJ, He F, Botros YY, et al. Mediating solar cell performance by controlling the internal dipole change in organic photovoltaic polymers. *Macromolecules* 2012;45:6390–5.

- [19] Stuart AC, Tumbleston JR, Zhou H, Li W, Liu S, Ade H, et al. Fluorine substituents reduce charge recombination and drive structure and morphology development in polymer solar cells. *J Am Chem Soc* 2013;135:1806–15.
- [20] Xiao Z, Subbiah J, Sun K, Ji S, Jones DJ, Holmes AB, et al. Thiazolyl substituted benzodithiophene copolymers: synthesis, properties and photovoltaic applications. *J Mater Chem C* 2014;2:1306–13.
- [21] Marsh RA, Groves C, Greenham NC. A microscopic model for the behavior of nanostructured organic photovoltaic devices. *J Appl Phys* 2007;101:083509.
- [22] Deibel C, Strobel T, Dyakonov V. Origin of the efficient polaron-pair dissociation in polymer-Fullerene blends. *Phys Rev Lett* 2009;103:036402.
- [23] Shen S, Jiang P, He C, Zhang J, Shen P, Zhang Y, et al. Solution-processable organic molecule photovoltaic materials with bithienyl-benzodithiophene central unit and indenedione end groups. *Chem Mater* 2013;25:2274–81.
- [24] Cheng M, Chen C, Yang X, Huang J, Zhang F, Xu B, et al. Novel small molecular materials based on phenoxazine core unit for efficient bulk heterojunction organic solar cells and perovskite solar cells. *Chem Mater* 2015;27:1808–14.
- [25] Li Z, He G, Wan X, Liu Y, Zhou J, Long G, et al. Solution processable rhodanine-based small molecule organic photovoltaic cells with a power conversion efficiency of 6.1%. *Adv Energy Mater* 2012;2:74–7.
- [26] Ni W, Li MM, Liu F, Wan XJ, Feng HR, Kan B, et al. Dithienosilole-based small-molecule organic solar cells with an efficiency over 8%: investigation of the relationship between the molecular structure and photovoltaic performance. *Chem Mater* 2015;27:6077–84.

- [27] Zhang Q, Kan B, Liu F, Long G, Wan X, Chen X, et al. Small-molecule solar cells with efficiency over 9%. *Nat Photonics* 2015;9:35–41.
- [28] Wang J-L, Liu K-K, Yan J, Wu Z, Liu F, Xiao F, et al. Series of multifluorine substituted oligomers for organic solar cells with efficiency over 9% and fill factor of 0.77 by combination thermal and solvent vapor annealing. *J Am Chem Soc* 2016;138:7687–97.
- [29] Tamayo AB, Walker B, Nguyen T-Q. A low band gap, solution processable oligothiophene with a diketopyrrolopyrrole core for use in organic solar cells. *J Phys Chem C* 2008;112:11545–51.
- [30] Liu J, Sun Y, Moonsin P, Kuik M, Proctor CM, Lin J, et al. Tri-diketopyrrolopyrrole molecular donor materials for high-performance solution-processed bulk heterojunction solar cells. *Adv Mater* 2013;25:5898–903.
- [31] Li Y, Sonar P, Murphy L, Hong W. High mobility diketopyrrolopyrrole (DPP)-based organic semiconductor materials for organic thin film transistors and photovoltaics. *Energy Environ Sci* 2013;6:1684–710.
- [32] Zhang Y, Xiao M, Su N, Zhong J, Tan H, Wang Y, et al. Efficient strategies to improve photovoltaic performance of linear-shape molecules by introducing large planar aryls in molecular center and terminals. *Org Electron* 2015;17:198–207.
- [33] Huang Y, Li L, Peng X, Peng J, Cao Y. Solution processed small molecule bulk heterojunction organic photovoltaics based on a conjugated donor–acceptor porphyrin. *J Mater Chem* 2012;22:21841–4.
- [34] Qin H, Li L, Guo F, Su S, Peng J, Cao Y, et al. Solution-processed bulk heterojunction solar cells based on a porphyrin small molecule with 7% power conversion efficiency. *Energy*

- Environ Sci 2014;7:1397–401.
- [35] Gao K, Li L, Lai T, Xiao L, Huang Y, Huang F, et al. Deep absorbing porphyrin small molecule for high-performance organic solar cells with very low energy losses. *J Am Chem Soc* 2015;137:7282–5.
- [36] Gao K, Miao J, Xiao L, Deng W, Kan Y, Liang T, et al. Multi-length-scale morphologies driven by mixed additives in porphyrin-based organic photovoltaics. *Adv Mater* 2016;28:4727–33.
- [37] Zhang Y, Xiao Y, Xie Y, Zhu L, Shi D, Cheng C. Fluorene-centered perylene monoimides as potential non-fullerene acceptor in organic solar cells. *Org Electron* 2015;21:184–91.
- [38] Loudet A, Burgess K. BODIPY dyes and their derivatives: synthesis and spectroscopic properties. *Chem Rev* 2007;107:4891–932.
- [39] Ulrich G, Ziessel R, Harriman A. The chemistry of fluorescent bodipy dyes: versatility unsurpassed. *Angew Chem Int Ed* 2008;47:1184–201.
- [40] Qin W, Leen V, Dehaen W, Cui J, Xu C, Tang X, et al. 3,5-Dianilino substituted difluoroboron dipyrromethene: synthesis, spectroscopy, photophysics, crystal structure, electrochemistry, and quantum-chemical calculations. *J Phys Chem C* 2009;113:11731–40.
- [41] Leen V, Miscoria D, Yin S, Filarowski A, Molisho Ngongo J, Van der Auweraer M, et al. 1,7-Disubstituted boron dipyrromethene (BODIPY) dyes: synthesis and spectroscopic properties. *J Org Chem* 2011;76:8168–76.
- [42] Liao J, Wang Y, Xu Y, Zhao H, Xiao X, Yang X. Synthesis, optical and electrochemical properties of novel meso-triphenylamine-BODIPY dyes with aromatic moieties at 3,5-positions. *Tetrahedron* 2015;71: 5078–84.

- [43] Liao J, Xu Y, Zhao H, Wang Y, Zhang W, Peng F, et al. Synthesis, optical, electrochemical properties and photovoltaic performance of novel panchromatic meso-thiophene BODIPY dyes with a variety of electron-donating groups at the 3,5-positions. *RSC Adv* 2015;5:86453–62.
- [44] Rousseau T, Cravino A, Bura T, Ulrich G, Ziessel R, Roncali J. BODIPY derivatives as donor materials for bulk heterojunction solar cells. *Chem Commun* 2009;1673–5.
- [45] Lin H-Y, Huang W-C, Chen Y-C, Chou H-H, Hsu C-Y, Lin JT, et al. BODIPY dyes with β -conjugation and their applications for high-efficiency inverted small molecule solar cells. *Chem Commun* 2012;48:8913–5.
- [46] Bura T, Leclerc N, Fall S, L  v  que P, Heiser T, Retailleau P, et al. High-performance solution-processed solar cells and ambipolar behavior in organic field-effect transistors with thienyl-BODIPY scaffoldings. *J Am Chem Soc* 2012;134:17404–7.
- [47] Liu W, Tang A, Chen J, Wu Y, Zhan C, Yao J. Photocurrent enhancement of BODIPY-based solution-processed small-molecule solar cells by dimerization via the meso position. *ACS Appl Mater Interfaces* 2014;6: 22496–505.
- [48] Xiao L, Wang H, Gao K, Li L, Liu C, Peng X, et al. A-D-A type small molecules based on boron dipyrromethene for solution-processed organic solar cells. *Chem Asian J* 2015;10:1513–8.
- [49] Zhang X, Zhang Y, Chen L, Xiao Y. Star-shaped carbazole-based BODIPY derivatives with improved hole transportation and nearinfrared absorption for small-molecule organic solar cells with high open-circuit voltages. *RSC Adv* 2015;5:32283–9.
- [50] Liao J, Zhao H, Xu Y, Cai Z, Peng Z, Zhang W, et al. Novel D-A-D type dyes based on

- BODIPY platform for solution processed organic solar cells. *Dyes Pigments* 2016;128:131–40.
- [51] Jadhav T, Misra R, Biswas S, Sharma GD. Bulk heterojunction organic solar cells based on carbazole–BODIPY conjugate small molecules as donors with high open circuit voltage. *Phys Chem Chem Phys* 2015;17:26580–8.
- [52] Bulut I, Huahlmé Q, Mirloup A, Chávez P, Fall S, Hébraud A, et al. Rational engineering of BODIPY-bridged trisindole derivatives for solar cell applications. *ChemSusChem* 2017;10:1878–82.
- [53] Guo X, Baumgarten M, Müllen K. Designing π -conjugated polymers for organic electronics. *Prog Polym Sci* 2013;38:1832–908.
- [54] Yao HF, Ye L, Zhang H, Li SS, Zhang SQ, Hou JH. Molecular design of benzodithiophene-based organic photovoltaic materials. *Chem Rev* 2016;116:7397–457.
- [55] Hua Y, Chang S, Huang D, Zhou X, Zhu X, Zhao J, et al. Significant improvement of dye-sensitized solar cell performance using simple phenothiazine-based dyes. *Chem Mater* 2013;25:2146–53.
- [56] Hou J, Chen H-Y, Zhang S, Chen RI, Yang Y, et al. Synthesis of a low band gap polymer and its application in highly efficient polymer solar cells. *J Am Chem Soc* 2009;131:15586–7.
- [57] Ma X, Azeem EA, Liu X, Cheng Y, Zhu C. Synthesis and tunable chiroptical properties of chiral BODIPY-based D–p–A conjugated polymers. *J Mater Chem C* 2014;2:1076–84.
- [58] Khan MS, Al-Mandhary MRA, Al-Suti MK, Ahrens B, Mahon MF, Male L, et al. Synthesis, characterisation and optical spectroscopy of diynes and poly-ynes containing derivatised fluorenes in the backbone. *Dalton Trans* 2003;74–84.
- [59] Popere BC, Della Pelle AM, Poe A, Balaji G, Thayumanavan S. Predictably tuning the

frontier molecular orbital energy levels of panchromatic low band gap BODIPY-based conjugated polymers. *Chem Sci* 2012;3:3093–102.

[60] Maglione C, Carella A, Centore R, Chávez P, Lévêque P, Fall S, et al. Novel low bandgap phenothiazine functionalized DPP derivatives prepared by direct heteroarylation: Application in bulk heterojunction organic solar cells. *Dye Pigment* 2017;141:169-78.

[61] Tan Q, Yang X, Cheng M, Wang H, Wang X, Sun L. Application of small molecule donor materials based on phenothiazine core unit in bulk heterojunction solar cells. *J Phys Chem C* 2014;118:16851–5.

[62] Malliaras GG, Salem JR, Brock PJ, Scott C. Electrical characteristics and efficiency of single-layer organic light-emitting diodes. *Phys Rev B* 1998;58:13411–4.

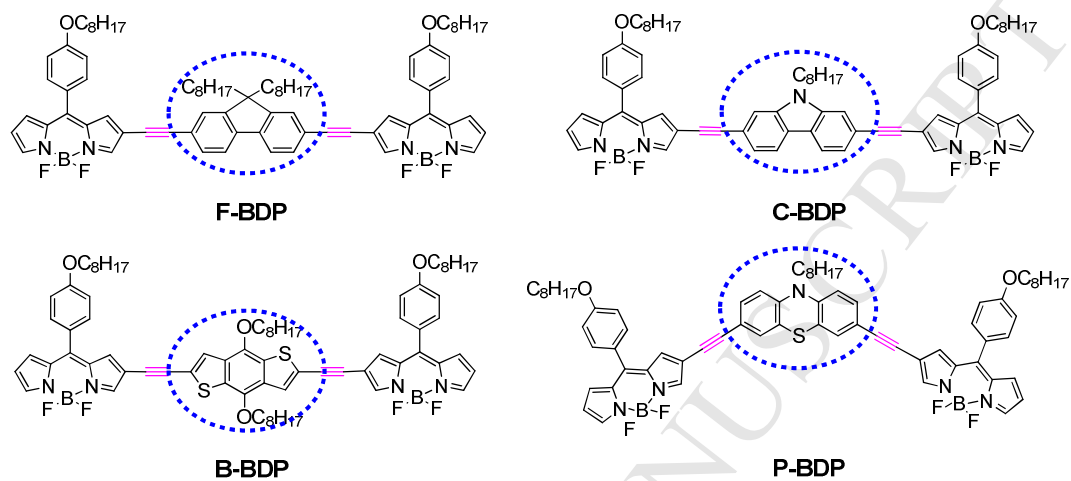
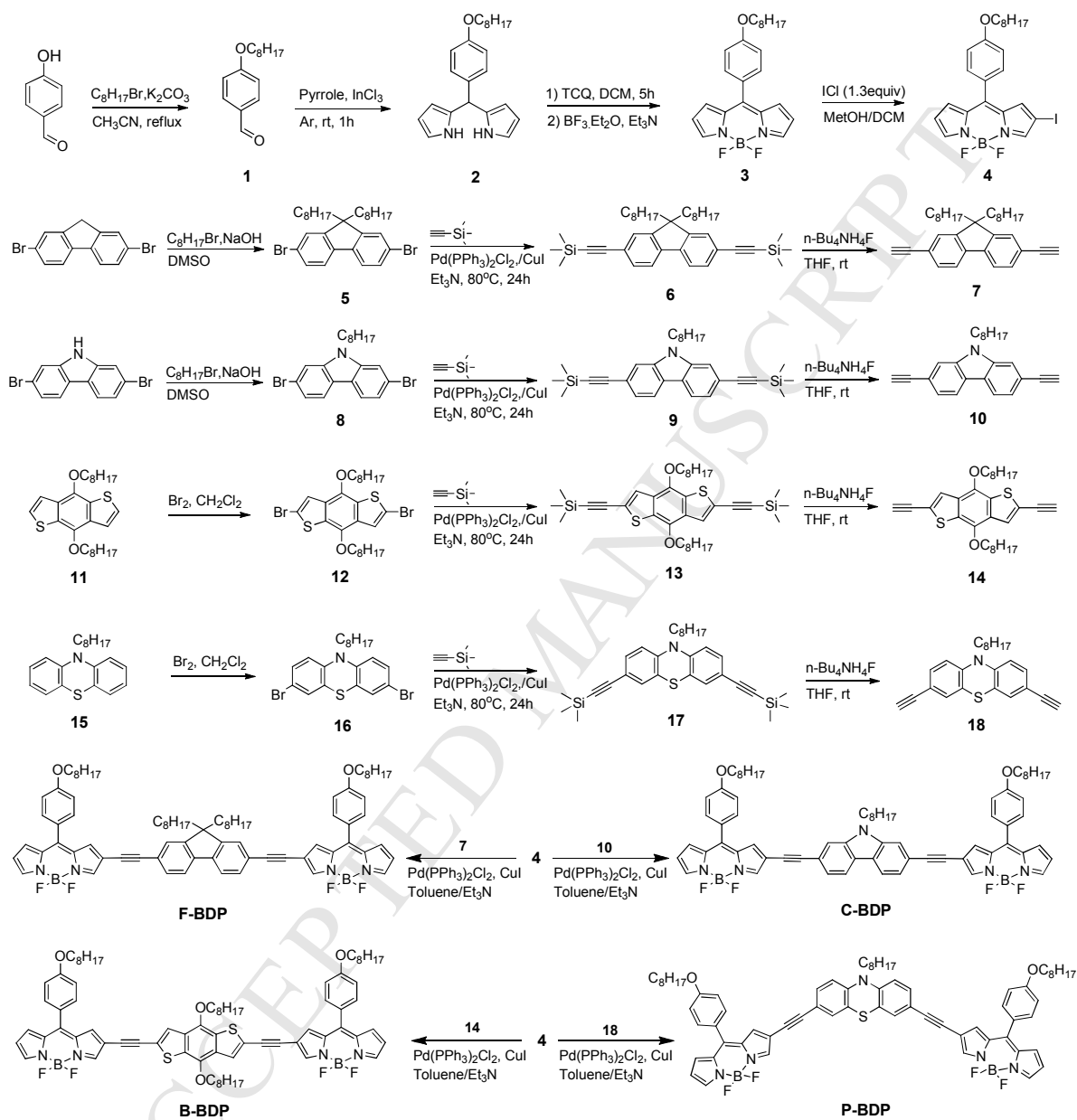


Chart 1. The molecular structure of SMs: **F-BDP**, **C-BDP**, **B-BDP** and **P-BDP**.



Scheme 1. Synthetic routes of F-BDP, C-BDP, B-BDP and P-BDP.

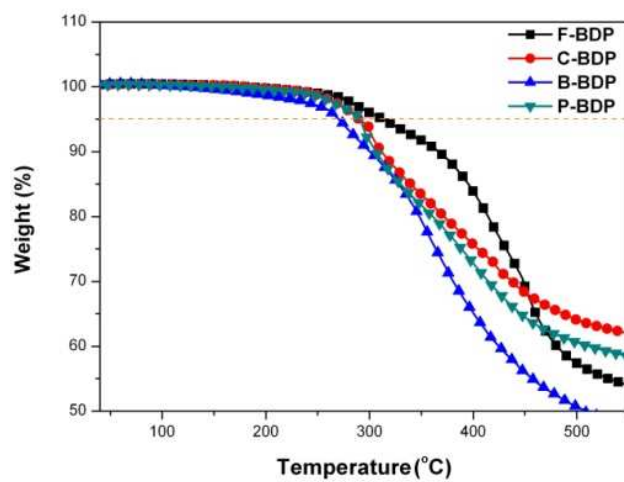


Fig. 1. The TGA curves of F-BDP, C-BDP, B-BDP and P-BDP.

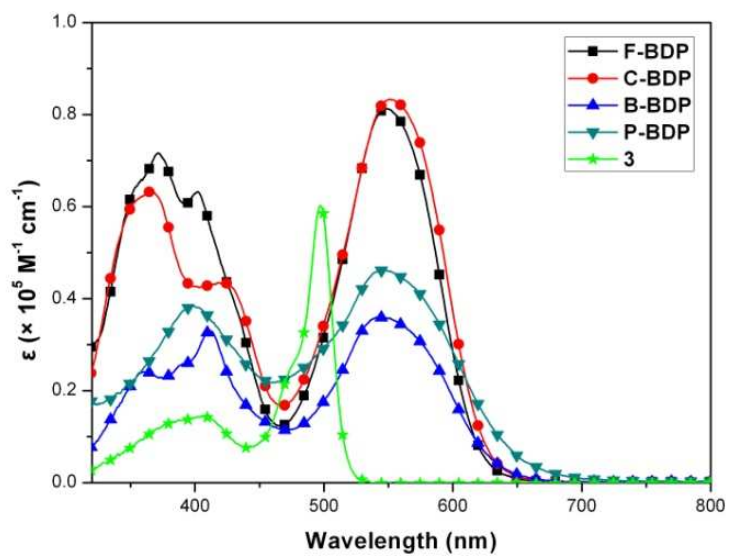


Fig. 2. UV-vis absorption spectra of 3, F-BDP, C-BDP, B-BDP and P-BDP in CH_2Cl_2 solution.

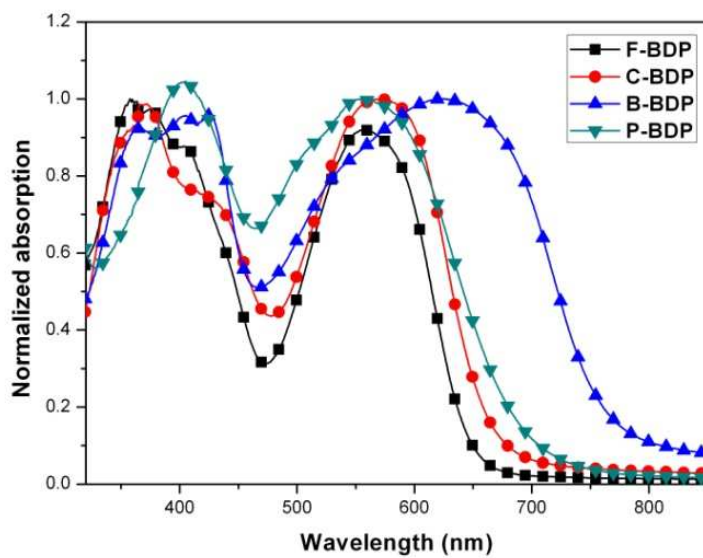


Fig. 3. Normalized UV-vis absorption spectra of **F-BDP**, **C-BDP**, **B-BDP** and **P-BDP** in films.

Table 1 Optical data for BODIPY **3**, **F-BDP**, **C-BDP**, **B-BDP** and **P-BDP**.

Entries	$\lambda_{\max}^{\text{abs}}$ (nm) ^a	ϵ_{\max} (cm ⁻¹ M ⁻¹)	$\lambda_{\max}^{\text{abs}}$ (nm) ^b	$\lambda_{\max}^{\text{em}}$ (nm) ^a	Stokes shift (nm)	Φ_f	T _d (°C)
3	498	0.59×10 ⁵	-	-	-	0.91	-
F-BDP	552	0.82×10 ⁵	565	632	80	0.05	314
C-BDP	554	0.84×10 ⁵	576	643	89	0.02	300
B-BDP	550	0.37×10 ⁵	641	624	74	0.02	295
P-BDP	548	0.47×10 ⁵	564	603	55	0.03	301

^a measured in CH₂Cl₂ solution. ^b measured in the neat film.

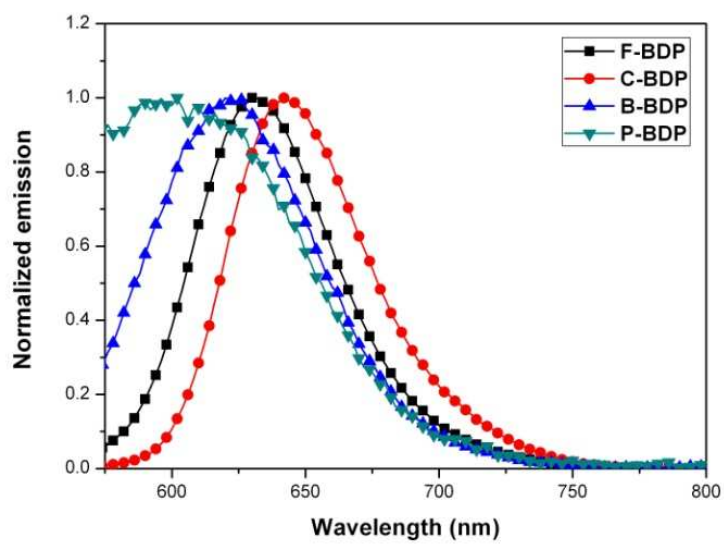


Fig. 4 Normalized fluorescence emission spectra of **F-BDP**, **C-BDP**, **B-BDP** and **P-BDP** in CH_2Cl_2 solution.

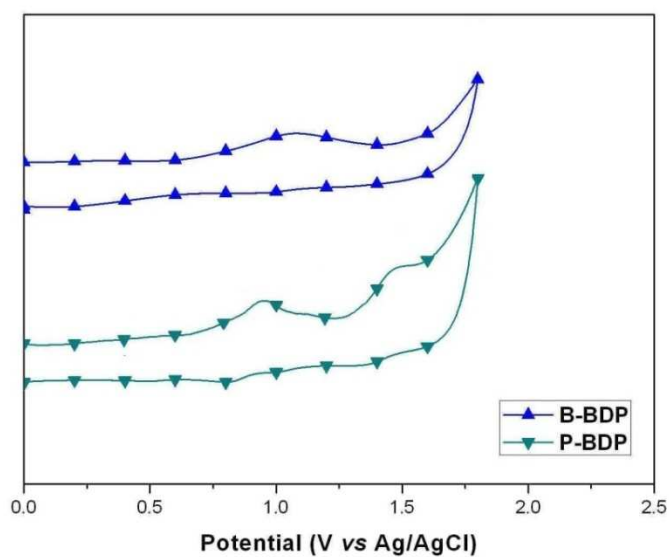
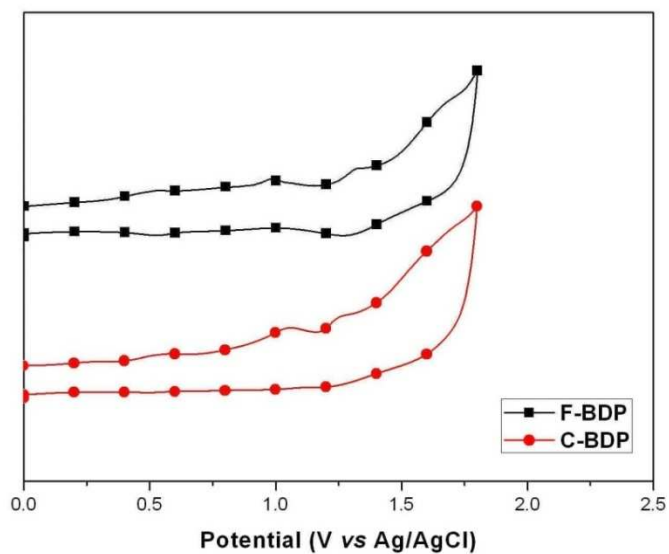


Fig. 5 Cyclic voltammograms of **F-BDP**, **C-BDP**, **B-BDP** and **P-BDP** in a CH_2Cl_2 solution of $0.1 \text{ mol L}^{-1} \text{ Bu}_4\text{NPF}_6$ at a scan rate of 100 mV s^{-1} .

Table 2 Electrochemical data for BODIPY 3, F-BDP, C-BDP, B-BDP and P-BDP.

Entries	E_g^a (eV)	$E_{\text{onset}}^{\text{ox}b}$ (V)	E_{red}^c (V)	HOMO ^d (eV)	LUMO ^d (eV)
F-BDP	1.85	0.96	-0.89	-5.24	-3.39
C-BDP	1.72	0.90	-0.82	-5.18	-3.46
B-BDP	1.46	0.83	-0.63	-5.11	-3.65
P-BDP	1.65	0.74	-0.91	-5.02	-3.37

^a E_g , estimated from the absorption thresholds from absorption spectra, $E_g = 1240/\lambda_{\text{onset}}$.

^b $E_{\text{onset}}^{\text{ox}}$, onset oxidation potential

^c E_{red} , the reduction potential, calculated from $E_{\text{onset}}^{\text{ox}} - E_g$.

^d $E_{\text{HOMO}} = [-(E_{\text{onset}}^{\text{ox}} - 0.52) - 4.8]$ eV, $E_{\text{LUMO}} = E_{\text{HOMO}} + E_g$ eV.

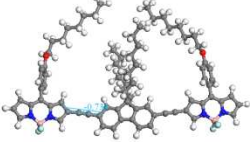
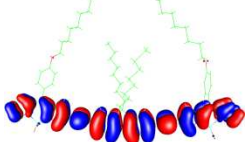
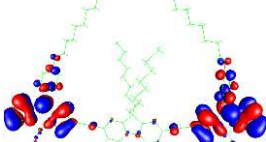
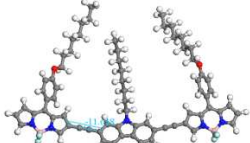
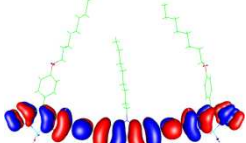
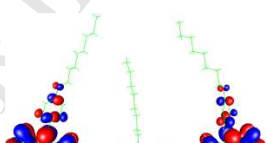
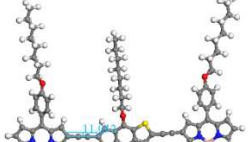
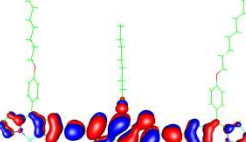
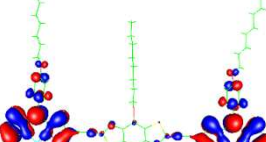
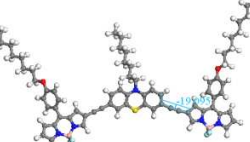
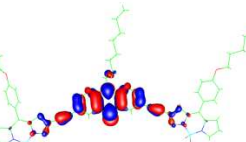
Entry	Optimized Structures	HOMO	Gap	LUMO
F-BDP	 $\Phi = 0.734$	 -5.323	2.199	 -3.125
C-BDP	 $\Phi = 11.638$	 -5.312	2.186	 -3.126
B-BDP	 $\Phi = 11.032$	 -5.162	1.987	 -3.175
P-BDP	 $\Phi = 19.095$	 -5.049	1.980	 -3.068

Fig. 6. The optimum geometries and the electron-state-density distributions of LUMO and HOMO

of F-BDP, C-BDP, B-BDP and P-BDP.

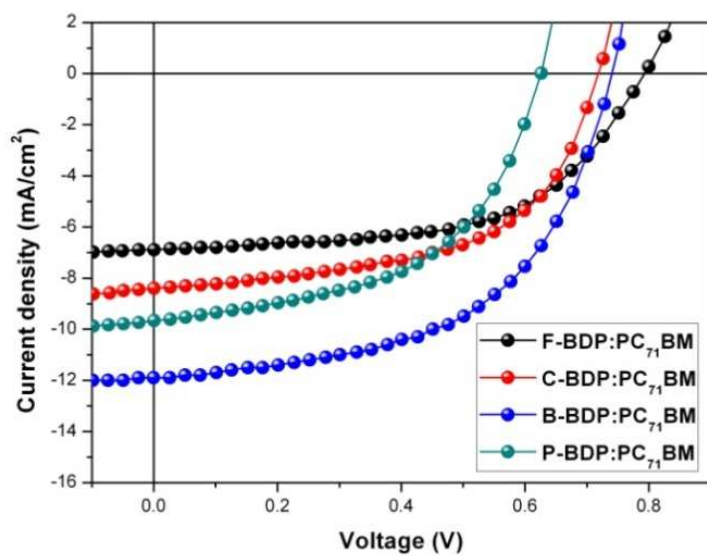


Fig. 7. Current density–voltage characteristics of **F-BDP**, **C-BDP**, **B-BDP**, and **P-BDP/PC₇₁BM** based OSCs under the optimized conditions under illumination of AM 1.5G, 100 mW·cm⁻².

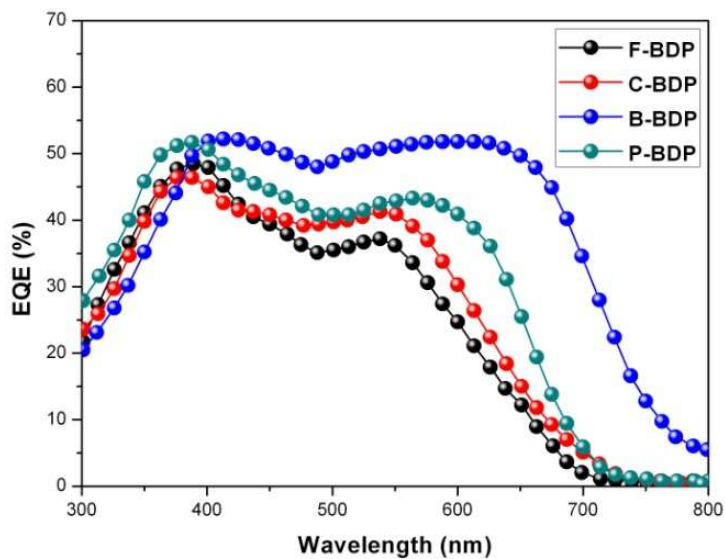


Fig. 8. External quantum efficiency curves of the devices based on **F-BDP**, **C-BDP**, **B-BDP**, and **P-BDP/PC₇₁BM** under the optimized conditions.

Table 3 Photovoltaic parameters of the optimized SMs:PC₇₁BM-based solar cells.

SMs	J_{sc}^a (mA cm ⁻²)	V_{oc} [V]	FF (%)	PCE (%) max/av^b	J_{sc}^c (mA cm ⁻²)	Hole mobility (cm ² V ⁻¹ s ⁻¹)
F-BDP	6.93	0.79	47.5	2.60 (2.58)	6.46	9.61×10^{-5}
C-BDP	8.37	0.72	50.1	3.02 (2.98)	8.01	1.34×10^{-4}
B-BDP	11.84	0.73	53.8	4.65 (4.61)	11.27	4.53×10^{-4}
P-BDP	9.76	0.63	54.1	3.33 (3.30)	9.22	3.11×10^{-4}

^a J_{sc} measured from solar cells.

^b Average values calculated from 8 devices.

^c J_{sc} estimated from EQE spectra.

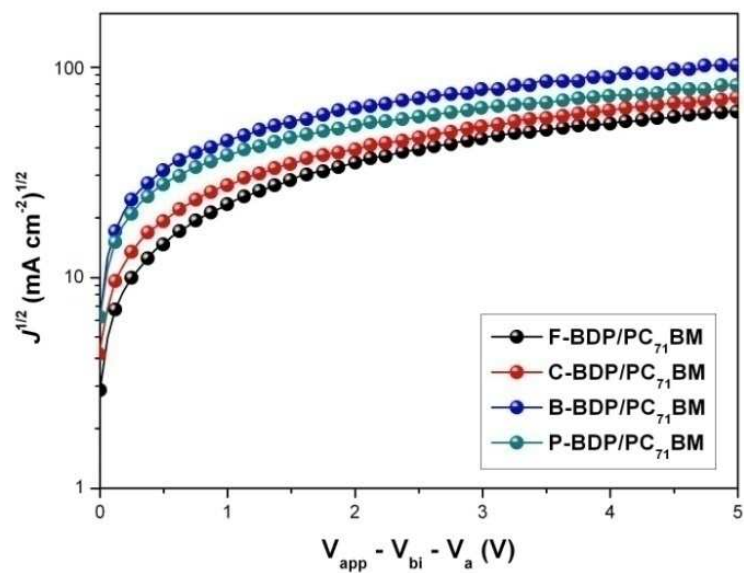


Fig. 9 J - V curves of the optimized hole-only SMs/PC₇₁BM devices.

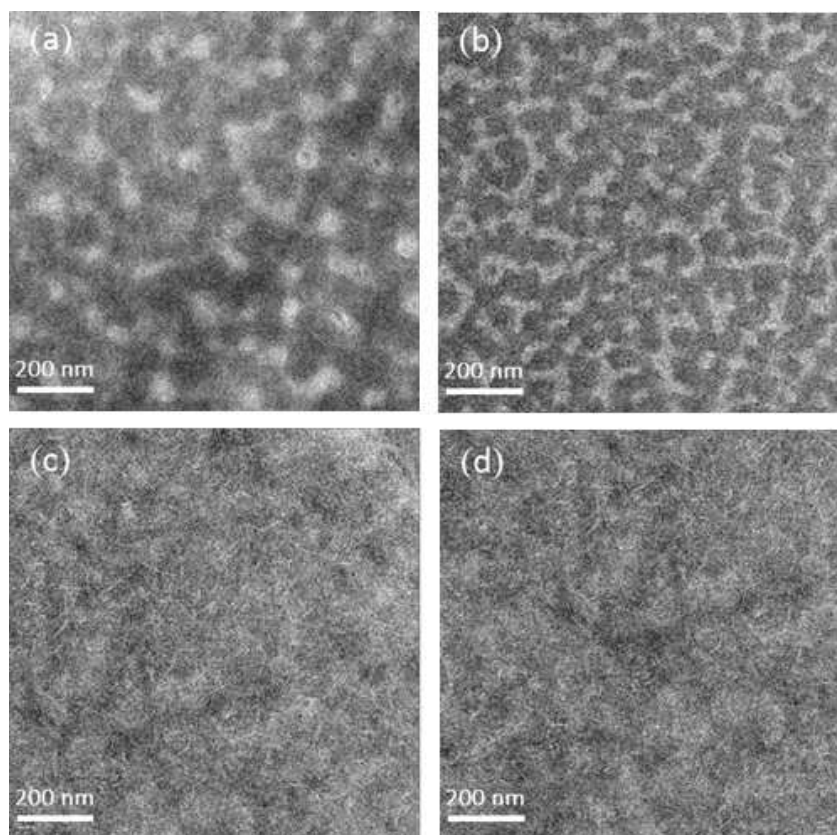


Fig. 10. TEM images of the blend films of (a) **F-BDP/PC₇₁BM**, (b) **C-BDP/PC₇₁BM**, (c) **B-BDP/PC₇₁BM**, and (d) **P-BDP/PC₇₁BM** under the optimized condition. The scale bar is 200 nm.

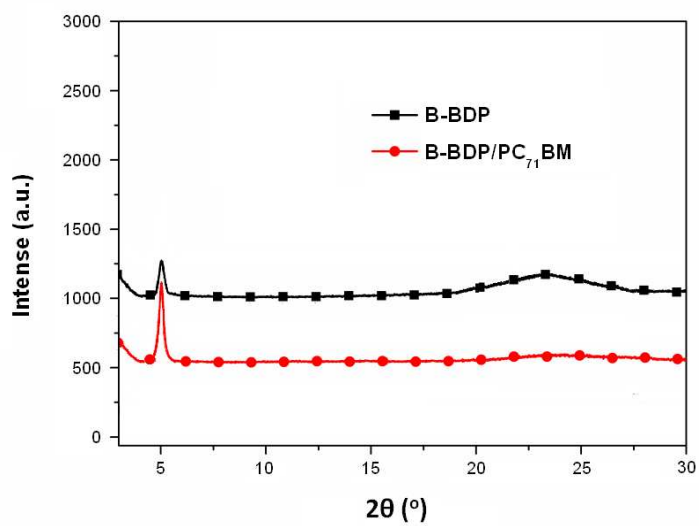


Fig. 11. XRD patterns of **B-BDP** film and **B-BDP/PC₇₁BM** film under the optimized conditions.

Chart 1. The molecular structures of SMs: **F-BDP**, **C-BDP**, **B-BDP** and **P-BDP**.

Scheme 1. Synthetic routes of **F-BDP**, **C-BDP**, **B-BDP** and **P-BDP**.

Fig. 1. The TGA curves of **F-BDP**, **C-BDP**, **B-BDP** and **P-BDP**.

Fig. 2. UV-vis absorption spectra of **3**, **F-BDP**, **C-BDP**, **B-BDP** and **P-BDP** in CH₂Cl₂ solution.

Fig. 3. Normalized UV-vis absorption spectra of **F-BDP**, **C-BDP**, **B-BDP** and **P-BDP** in films.

Table 1 Optical data for BODIPY **3**, **F-BDP**, **C-BDP**, **B-BDP** and **P-BDP**.

Fig. 4 Normalized fluorescence emission spectra of **F-BDP**, **C-BDP**, **B-BDP** and **P-BDP** in CH₂Cl₂ solution.

Fig. 5 Cyclic voltammograms of **F-BDP**, **C-BDP**, **B-BDP** and **P-BDP** in a CH₂Cl₂ solution of 0.1 mol L⁻¹ Bu₄NPF₆ at a scan rate of 100 mV s⁻¹.

Table 2 Electrochemical data for BODIPY **3**, **F-BDP**, **C-BDP**, **B-BDP** and **P-BDP**.

Fig. 6. The optimum geometries and the electron-state-density distributions of LUMO and HOMO of **F-BDP**, **C-BDP**, **B-BDP** and **P-BDP**.

Fig. 7. Current density–voltage characteristics of **F-BDP**, **C-BDP**, **B-BDP**, and **P-BDP/PC₇₁BM** based OSCs under the optimized conditions under illumination of AM 1.5G, 100 mW·cm⁻².

Fig. 8. External quantum efficiency curves of the devices based on **F-BDP**, **C-BDP**, **B-BDP**, and **P-BDP/PC₇₁BM** under the optimized conditions.

Table 3 Photovoltaic parameters of the optimized SMs:PC₇₁BM-based solar cells.

Fig. 9. *J-V* curves of the optimized hole-only SMs/PC₇₁BM devices.

Fig. 10. TEM images of the blend films of (a) **F-BDP/PC₇₁BM**, (b) **C-BDP/PC₇₁BM**, (c) **B-BDP/PC₇₁BM**, and (d) **P-BDP/PC₇₁BM** under the optimized condition. The scale bar is 200 nm.

Fig. 11. XRD patterns of **B-BDP** film and **B-BDP/PC₇₁BM** film under the optimized conditions.

Highlight:

- The novel BODIPY derivatives exhibited coplanar molecular structure due to the introduction of ethynyl bridges.
- These derivatives showed broad absorption covering from 300 to 900 nm with high ϵ , low fluorescent quantum yields and relatively low-lying HOMO energy levels.
- The **B-BDP**/PCBM based OSC exhibited an appealing PCE of 4.65% with a high J_{sc} of 11.84 mA cm⁻² and a high FF of 53.8%.